NASA/TM—2019-220071

Development and Characterization of Hot-Pressed Matrices for Engineered Ceramic Matrix Composites (E-CMCs)

S.V. Raj
Glenn Research Center, Cleveland, Ohio

March 2019

NASA STI Program . . . in Profile

Since its founding, NASA has been dedicated to the advancement of aeronautics and space science. The NASA Scientific and Technical Information (STI) Program plays a key part in helping NASA maintain this important role.

The NASA STI Program operates under the auspices of the Agency Chief Information Officer. It collects, organizes, provides for archiving, and disseminates NASA's STI. The NASA STI Program provides access to the NASA Technical Report Server—Registered (NTRS Reg) and NASA Technical Report Server—Public (NTRS) thus providing one of the largest collections of aeronautical and space science STI in the world. Results are published in both non-NASA channels and by NASA in the NASA STI Report Series, which includes the following report types:

- TECHNICAL PUBLICATION. Reports of completed research or a major significant phase of research that present the results of NASA programs and include extensive data or theoretical analysis. Includes compilations of significant scientific and technical data and information deemed to be of continuing reference value. NASA counter-part of peer-reviewed formal professional papers, but has less stringent limitations on manuscript length and extent of graphic presentations.

- TECHNICAL MEMORANDUM. Scientific and technical findings that are preliminary or of specialized interest, e.g., "quick-release" reports, working papers, and bibliographies that contain minimal annotation. Does not contain extensive analysis.

- CONTRACTOR REPORT. Scientific and technical findings by NASA-sponsored contractors and grantees.

- CONFERENCE PUBLICATION. Collected papers from scientific and technical conferences, symposia, seminars, or other meetings sponsored or co-sponsored by NASA.

- SPECIAL PUBLICATION. Scientific, technical, or historical information from NASA programs, projects, and missions, often concerned with subjects having substantial public interest.

- TECHNICAL TRANSLATION. English-language translations of foreign scientific and technical material pertinent to NASA's mission.

For more information about the NASA STI program, see the following:

- Access the NASA STI program home page at http://www.sti.nasa.gov

- E-mail your question to help@sti.nasa.gov

- Fax your question to the NASA STI Information Desk at 757-864-6500

- Telephone the NASA STI Information Desk at 757-864-9658

- Write to:
  NASA STI Program
  Mail Stop 148
  NASA Langley Research Center
  Hampton, VA 23681-2199

NASA/TM—2019-220071

Development and Characterization of Hot-Pressed Matrices for Engineered Ceramic Matrix Composites (E-CMCs)

S.V. Raj
Glenn Research Center, Cleveland, Ohio

National Aeronautics and
Space Administration

Glenn Research Center
Cleveland, Ohio 44135

March 2019

Acknowledgments

The author thanks Mr. Robert Angus, Mr. Raymond Babuder, Mr. Ronald Phillips, Ms. Joy Buehler, and Mr. Terry McCue for their assistance. Funding for this research was provided by NASA's ARMD Seedling Fund Phases I & II, and this is gratefully acknowledged.

This paper was published in the Journal Ceramic International, Volume 45, Issue 3, 15 February 2019, pp. 3608–3619, Elsevier and can be found at https://doi.org/10.1016/j.ceramint.2018.11.021.

Level of Review: This material has been technically reviewed by technical management.

Available from

NASA STI Program
Mail Stop 148
NASA Langley Research Center
Hampton, VA 23681-2199

National Technical Information Service
5285 Port Royal Road
Springfield, VA 22161
703-605-6000

This report is available in electronic form at http://www.sti.nasa.gov/ and http://ntrs.nasa.gov/

Development and Characterization of Hot-Pressed Matrices for Engineered Ceramic Matrix Composites (E-CMCs)

S.V. Raj
National Aeronautics and Space Administration
Glenn Research Center
Cleveland, Ohio 44135

Abstract

The present research effort was undertaken to develop a new generation of SiC fiber- reinforced engineered ceramic matrix composites (E-CMCs). In contrast to traditional CMCs with a brittle SiC matrix, an E-CMC is designed to consist of a matrix engineered to possess sufficient high temperature plasticity to minimize crack propagation, relatively high fracture toughness, and self-healing capabilities to prevent oxygen ingress to the BN-coated fibers through surface-connected cracks. The present paper discusses the bend strength, isothermal oxidation, microstructures and self-healing properties of several silicide-behaved engineered matrices. Based on the oxidation tests, where it was observed that some of the matrices exhibited either catastrophic oxidation ("pesting") or spalling of the oxide scale, two engineered matrices, $CrSi_2$/SiC/Si_3N_4 and a CrMoSi/SiC/Si_3N_4, were down-selected for further investigation. Four-point bend tests were conducted on these two engineered matrices between room temperature and 1698 K. Although these matrices were brittle at low temperatures, it was observed that the bend strengths and bend ductility increased at high temperatures as the silicide particles became more ductile, which was qualitatively consistent with the theoretically expected behavior that crack blunting at these particles should increase the matrix strength. Additional studies were conducted to study the effects of different additives on the self-healing properties of the engineered matrices, which helped to identify the most effective additives.

1.0 Introduction

Silicon carbide fiber-reinforced ceramic matric composites (CMCs) are being developed for aerospace applications to replace Ni-based superalloys in gas turbine engines (Refs. 1 to 8). In contrast to Ni-based superalloys, replacement with lighter weight SiC/SiC_f CMCs are expected to allow several hot section components, such as combustor liners, shrouds, and turbine blades and vanes, to operate at higher temperatures and higher pressure ratios with reduced cooling air. In practical terms, the increased engine efficiency would result in lower fuel burn thereby leading to lower CO_2 emissions and significant cost savings in the operation of each aircraft. As a result of decades of research and development, SiC/SiC_f CMCs are finding applications in advanced aircraft engines (Ref. 9). However, a major deficiency with these CMCs is that the matrix has low toughness, where the design stresses, which are typically less than the tensile proportional stress of the CMC, are limited by a relatively low matrix cracking stress of less than 192 MPa (Refs. 6, 10 to 13). In particular, surface connected cracks critically limit the life of the composite since oxygen ingress to the BN coatings on fibers leads to the formation low melting borosilicate glass (Ref. 6). Additionally, moisture attack of the fibers and matrix also contributes to lower durability. If these CMCs are fabricated by Si melt infiltration, there is a possibility that the presence of unconverted residual Si (i.e., "free Si") would significantly limit the use temperature below that of the melting point of Si due to poor creep properties of the CMCs. Thus, the full potential of the high creep strength SiC_f in unlikely to be fulfilled in actual applications for these SiC/SiC_fCMCs.

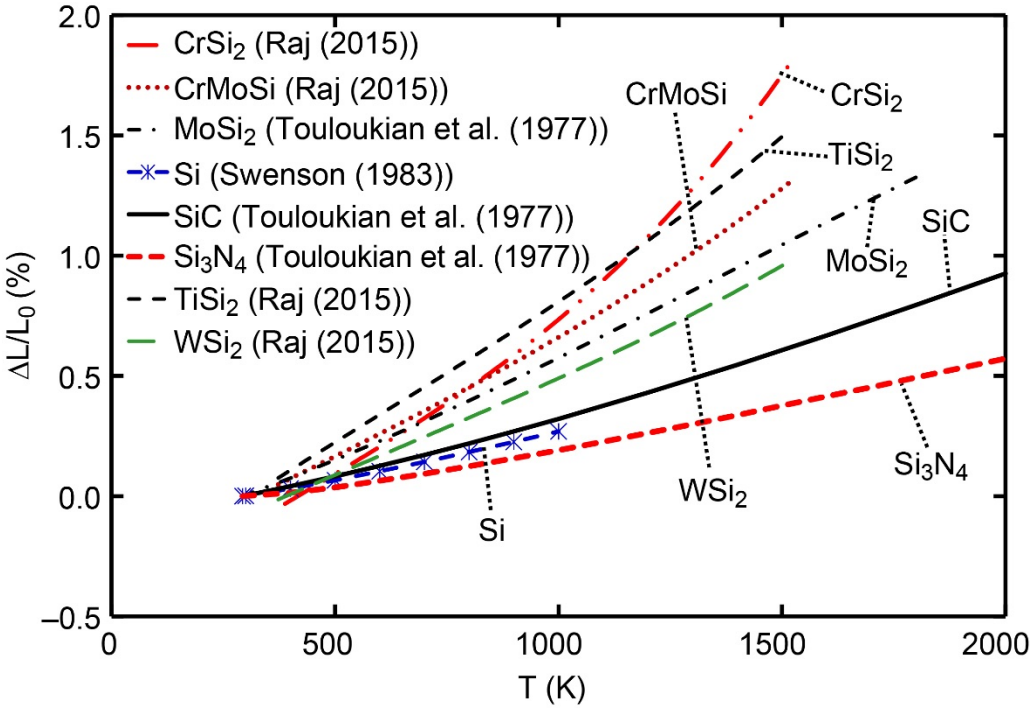

Figure 1.—Comparison of the temperature dependence of the average thermal expansion behavior of hot-pressed $CrSi_2$ (Ref. 17), Cr-30%Mo-30%Si (Ref. 17), $MoSi_2$ (Ref. 15), Si (Ref. 16), SiC (Ref. 15), Si_3N_4 (Ref. 15), $TiSi_2$ (Ref. 17) and WSi_2 (Ref. 17) between 293 and 2000 K.

Given these potential limitations, it is important to consider other approaches that may be necessary to develop CMCs for applications as high as 1482 °C (2700 °F). In principle, melt infiltration with a metal silicide with a higher melting point than pure Si would increase the use temperature of the CMC. However, as discussed in an earlier paper (Ref. 14), the thermal expansions of several common silicides are significantly higher than that of SiC, where the extent of deviation increases with increasing temperature (Fig. 1). The data shown in Figure 1 have been compiled from various sources (Refs. 15 to 17).

The design of an engineered matrix (EM) for a CMC with an increased durability for application above the melting point of Si must satisfy certain requirements. First, the thermal expansion of the engineered matrix should be close to that of the SiC_f fibers to minimize the amount of thermal strains developed during thermal fatigue. Second, all the constituents should be chemically stable and should not react with each other, the SiC_f, the BN coatings and CVI SiC. Third, the melting points of all the constituents should be above the intended application temperature of the CMC to prevent incipient melting and chemical reaction. Fourth, the design of the EM should include second phase particles, which are ductile over a wide range of temperatures but especially at the operating temperatures of the CMCs so that they are effective at blunting cracks and prevent their propagation through the matrix. Fifth, the addition of self-healing additives to the matrix constituents can heal surface-connected matrix cracks and prevent H_2O ingress into the CMC, thereby protecting the BN coatings and the SiC_f. It is envisioned that the engineered ceramic matrix composites (E-CMCs) would be fabricated by slurry infiltrating the engineered matrix into CMC preforms followed by melt infiltration with a silicide. This is important to ensure that there is no significant “free Si” present in the CMC, which could lead to poor creep properties.

In order to compensate for the observed differences in the thermal expansion between the silicides and SiC, Raj (Ref. 14) extended the concepts presented in previous studies (Refs. 18 and 19) by proposing a generalized predictive approach based on the rule of mixtures (ROM) given by Equation (1):

$$(\Delta L/L_0)_{fiber} = (\Delta L/L_0)_{EM} = V_1(\Delta L/L_0)_1 + V_2(\Delta L/L_0)_2 + V_3(\Delta L/L_0)_3 + \ldots \quad (1)$$

where $(\Delta L/L_0)_{fiber}$ is the thermal strain in the fiber, $(\Delta L/L_0)_{EM}$ is the thermal strain in the engineered matrix (EM), $(\Delta L/L_0)_i$ is thermal strain of the i^{th} constituent (i = 1,2,3…n), V_i is the volume fraction of the i^{th} constituent, and $\sum_{i=1}^{n} V_i = 1$. For a three-constituent engineered matrix consisting of a silicide, SiC and Si_3N_4, Equation (1) reduces to

$$(\Delta L/L_0)_{fiber} = (\Delta L/L_0)_{EM} = V_{silicide}(\Delta L/L_0)_{silicide} + V_{SiC}(\Delta L/L_0)_{SiC} + V_{Si3N4}(\Delta L/L_0)_{Si3N4} \quad (2)$$

Additional terms must be included if self-healing and other additives are added to the matrix. Equations (1) and (2) provide a simple way to balance out the thermal expansion differences between the different materials.

Referring to Figure 1 and Equation (2), for a three constituent EM consisting of a silicide, SiC and Si_3N_4, the high thermal expansion of the silicide has to be compensated by the low thermal expansion of Si_3N_4 in order to match the thermal expansion of SiC_f. In this case, the volume fraction of SiC in the traditional matrix is replaced by suitable amounts of silicides and Si_3N_4 to satisfy Equation (2) (Table 1) so that the thermal expansion of the engineered matrix is close to that of SiC_f. It is important to note that by suitably varying the relative amounts of the constituents so as to develop compressive stresses in the engineered matrix, the crack resistance ability of the engineered matrix can be enhanced. Figure 2 graphically illustrates the concept (Ref. 14). The validity of Equation (2) was demonstrated in an earlier paper (Fig. 3) (Ref. 14). It was shown that the thermal expansions of several compositions of engineered matrices formulated using Equation (2) were in close agreement with the thermal expansion of SiC between 373 and 1523 K. While ensuring that the thermal expansions of the EMs are similar to that of SiC is a necessary condition for designing a suitable matrix for a CMC, it is also important to establish that the oxidation properties are acceptable and the silicide particles have an ability to blunt cracks at temperatures above the ductile-to-brittle transition (DBTT) for the matrix to be truly useful. The objectives of the present paper are to characterize the isothermal oxidation, bend strength and self-healing properties of these engineered matrices to downselect the compositions for further development.

TABLE 1.—COMPARISON OF THE ENGINEERED AND TRADITIONAL MATRIX COMPOSITION IN A CERAMIC MATRIX COMPOSITE USING EQUATION (2)

Concept	$V_{silicide}$ (%)	V_{SiC} (%)	V_{Si3N4} (%)
Traditional matrix	0	100	0
Engineered matrix	x	100-x-y	y

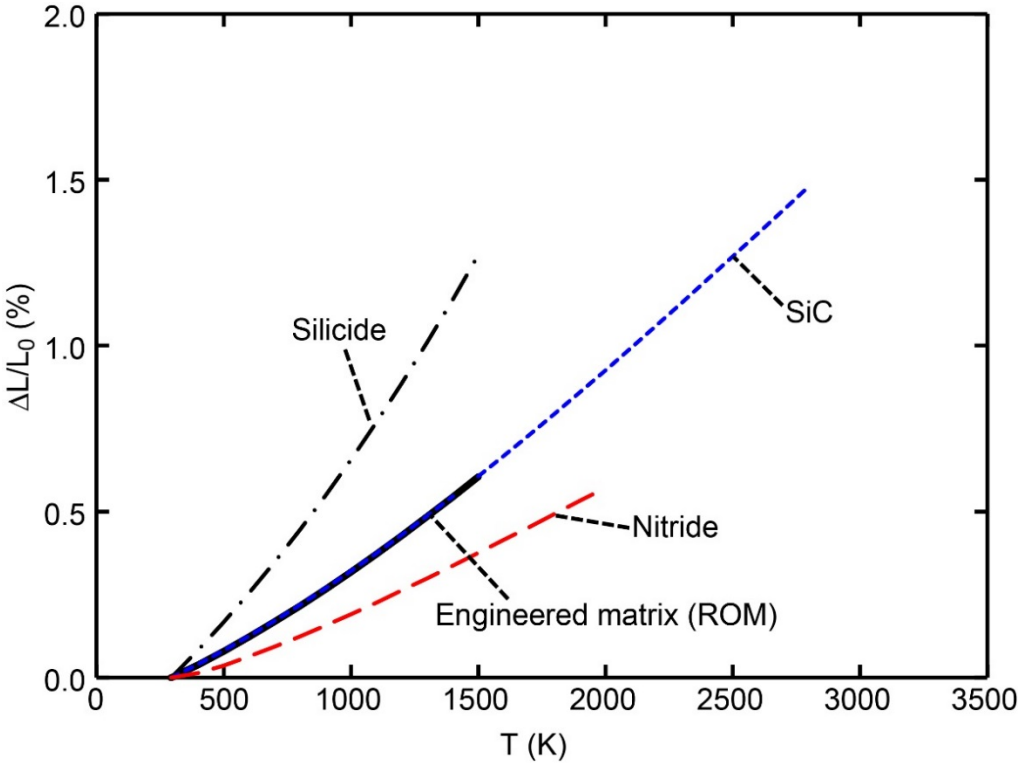

Figure 2.—Schematic illustration of the concept of engineering a matrix of a silicide, SiC and a nitride so as to match its thermal expansion with that of the SiC fibers (Ref. 14).

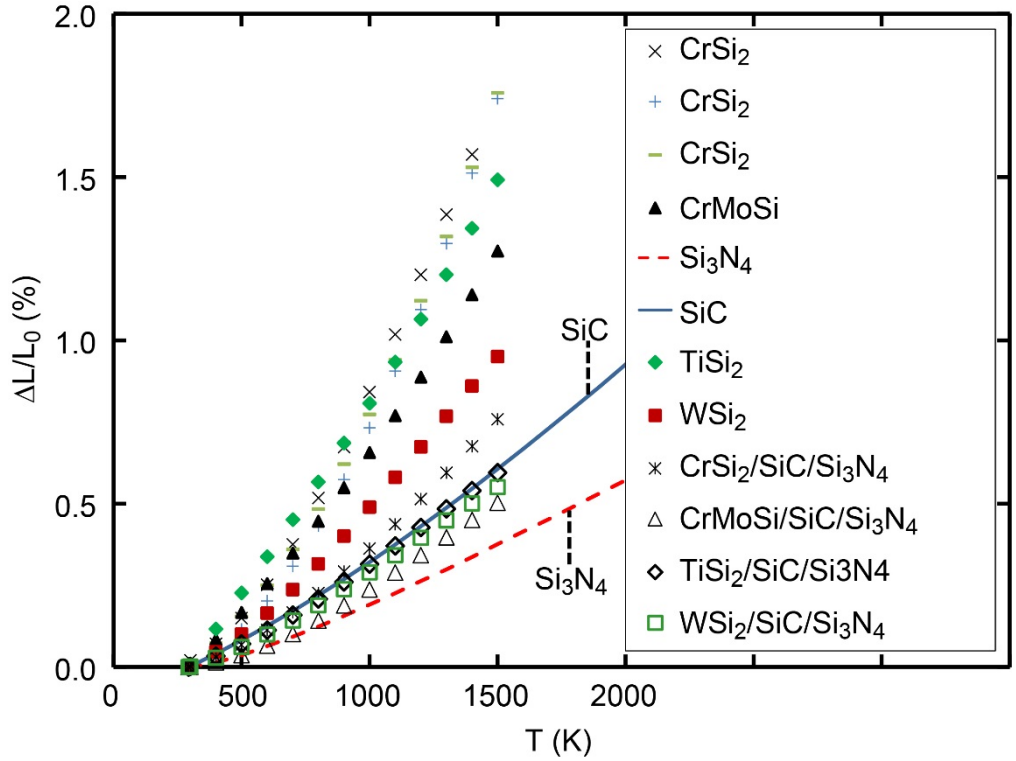

Figure 3.—Comparison of the temperature dependence of the thermal strains for disilicides (Ref. 17), CrMoSi (Ref. 17), engineered matrices (Ref. 14) with those for SiC (Ref. 15) and Si_3N_4 (Ref. 15).

2.0 Experimental Procedures

Details of the fabrication of the EMs studied in the present investigation are described elsewhere (Ref. 14). Briefly, the constituents used to fabricate EMs were high purity β-SiC (HSC059) submicron powders procured from the Superior Graphite Co., Chicago, IL, high purity Si_3N_4 (grade SN-E10) powders procured from Ube America, Inc., New York, N.Y, and commercial purity silicide powders (–325 mesh) of $CrSi_2$, $TiSi_2$, WSi_2 and a Cr-30(at.%)Mo-30%Si (CrMoSi) alloy (Refs. 20 to 24). The volume fractions of the individual constituents to formulate each SiC/Si_3N_4/silicide EM were determined using Equation (2), where the thermal expansion values for the SiC, Si_3N_4 and the silicides were obtained from literature sources (Refs. 16 and 17). The engineered compositions investigated in the present study were 10(vol.%)$CrSi_2$-70%SiC-20%Si_3N_4 ($CrSi_2$-EM), 10(vol.%)CrMoSi-60%SiC-30%Si_3N_4 (CrMoSi-EM), 10(vol.%)$MoSi_2$-70%SiC-20%Si_3N_4 ($MoSi_2$-EM), 10(vol.%)$TiSi_2$-70%SiC-20%Si_3N_4 ($TiSi_2$-EM) and 10(vol.%)WSi_2-70%SiC-20%Si_3N_4 (WSi_2-EM). These engineered matrix compositions did not have any self-healing additives. The Mo-50(vol.%) Si_3N_4 powder used in an earlier investigation (Ref. 19) was reformulated by adding appropriate amounts of SiC to form $MoSi_2$-EM.

The powders were wet ground in ethanol in a ball mill using SiC grinding media for 48 h. After grinding, the powders the excess alcohol was allowed to evaporate off and the wet powder cake was oven dried. The dried powder cakes were hand ground to powder using a mortar and pestle. The powders were hot-pressed under argon using SiC grinding media. After drying, the powder cakes were hand ground to fine powder in a mortar and pestle. The powders were hot-pressed to shape in graphite dies in either an argon or a nitrogen environment at temperatures varying between 1183 and 2073 K for times varying between 0.25 and 4 h. The hot pressing stresses varied between 69 and 105 MPa. Specimens were machined from the hot-pressed materials for microstructural evaluation, oxidation studies and four-point bend testing.

The nominal dimensions of the oxidation specimens were 13.5 mm in diameter and 3 mm thick. Each specimen had a 2.5 mm diameter hole machined by electro-discharge machining (EDM) about 3.2 mm from the edge to allow it to hang from a quartz hook in a thermogravimetric analyzer (TGA). The TGA was equipped with a weighing balance to periodically monitor the weight. The oxidation specimens were isothermally oxidized at 1600 K for 100 h in dry air flowing at 100 sccm. The data were logged by a computer data acquisition system.

Four-point bend tests were conducted on engineered matrices where the nominal specimen dimensions were 50 × 4 × 3 mm according to ASTM C 1161-02C (Ref. 25) and ASTM C 1211-13 (Ref. 26). These specimens were machined flat and parallel from hot-pressed plates nominally 50 × 50 × 3 mm in dimensions using a diamond saw. Bend tests were conducted in air between room temperature and 1698 K in a servo-hydraulic uniaxial testing machine at a crosshead speed, v, of 8.3×10^{-3} mm/s. The distance of the outer span, L_B, between the bottom rolls was 40 mm and that of the inner span, L_T, between the top rolls was 20 mm, where the distance, a, between the bottom and top roll was 10 mm. The center point displacement strain reported in this paper was calculated by the commercial software associated with the testing machine's data acquisition system from the cross-head deflection, δ. The center point strain rate, $\dot{\varepsilon}$, given by

$$\dot{\varepsilon} = \frac{12tv}{(3L_B^2 - 4a^2)} \tag{3}$$

where t is specimen thickness and a = L_B-L_T, was estimated to be 6.8×10^{-5} s^{-1} for t = 3 mm, v = 8.3×10^{-3} mm/s, L_B = 40 mm and a = 10 mm.

TABLE 2.—COMPOSITIONS OF DISKS WITH SELF-HEALING ADDITIVES IN WT.% AND OXIDATION HEAT TREATMENT CONDITIONS

Specimen I.D.	Compositions (wt.%)	Atm.	Temp. (K)	Hold time (h)
741-SiC-CMS	20%CrMoSi-80%SiC	Air	1600	24; 100
742-SiC-CMSY	20%CrMoSiY-80%SiC	Air	1600	24; 100
744-SiC-CMSGe	20%CrMoSiGe-80%SiC	Air	1600	24; 100
746-SiC-CMS-CB-1	20%CrMoSi-79%SiC-1%CrB_2	Air	1600	24; 100
748-SiC-CMS-CB-5	20%CrMoSi-75%SiC-5%CrB_2	Air	1600	24; 100
750-SiC-CMS-ZSO-1	20%CrMoSi-79%SiC -1%$ZrSiO_4$	Air	1600	24; 100
753-SiC-CMS-ZSO-5	20%CrMoSi-75%SiC-5%$ZrSiO_4$	Air	1600	24; 100
756-SiC-CS-CB-1	20%$CrSi_2$-79%SiC -1%CrB_2	Air	1600	24; 100
758-SiC-CS-CB-5	20%$CrSi_2$-75%SiC-5%CrB_2	Air	1600	24; 100
761-SiC-CS-ZSO-1	20%$CrSi_2$-79%SiC-1%$ZrSiO_4$	Air	1600	24; 100
763-SiC-CS-ZSO-5	20%$CrSi_2$-75%SiC-5%$ZrSiO_4$	Air	1600	24; 100

Note: These powders were hot-pressed under flowing Ar gas. The specimens were first oxidized for 24 h to conduct microstructural observations. The oxidation treatment was continued to a total time of 100 h. All specimens were heated at 0.4 K/s to the oxidation temperature and furnace cooled from this temperature.

Several $CrSi_2$/SiC and CrMoSi/SiC matrices were formulated without Si_3N_4 to study the effect of CrB_2, Ge, Y and $ZrSiO_4$ additives on self-healing of cracks and holes in order to downselect suitable self-healing additives. Table 2 gives details of the compositions in wt.%. The amount of CrB_2 and $ZrSiO_4$ were 1 and 5 wt.%, which were added as powders. In contrast, 1 wt.% Ge and 0.1 wt.% Y were present as solid solution in two batches of the gas atomized CrMoSi powders. These compositions were wet ball milled in ethanol as described previously and hot-pressed into disks 12.7 mm diameter and 3.2 mm thickness. A hole (~1 mm dia.)[1] was drilled on both faces of each specimen and polished on a 600 grit emery paper before annealing them in air in a rapid heating box furnace. The $CrSi_2$ and CrMoSi-based specimens were oxidized at 1600 and 1700 K, respectively, for a cumulative oxidation time of 100 h (Table 2). The oxidized specimens were microstructurally examined to study the extent of scratch healing and hole closure. Optical, scanning electron microscopy (SEM), back scattered electron (BSE) imaging and energy dispersive spectroscopy (EDS) were conducted of the specimen surfaces before and after oxidation by monitoring the extent of self-healing of the hole and scratches[2].

3.0 Results and Discussion

Details of the microstructures, and EDS and x-ray diffraction (XRD) analyses of the hot-pressed engineered matrices were described in great detail elsewhere (Ref. 14). Briefly, the microstructures of these specimens consisted of a distribution of coarser SiC particles intermixed with fine Si_3N_4 particles with the silicide particles variously distributed in the microstructure. The EDS showed C, N and O peaks in addition to Si and metallic peaks, which suggested the probable presence of silicon oxy-carb-nitride and oxy-nitride phases. There was some indication from the XRD quantitative phase analyses (QPA) results that there may have been some reaction between the silicides and SiC and Si_3N_4 particles but these observations could not be confirmed by EDS. The QPA results revealed that the volume fraction of the reacted phases varied from one composition to another but was less than 4.2 vol.% (Ref. 14). Owing to the complex nature of the XRD spectra, there was some uncertainty in conducting the Rietveld analysis

[1] It is noted that this is an approximate dimension of the hole diameter. In some instances, the actual hole diameter deviated by as much as 20% probably because the specimen porosity was very high, which made it difficult to precisely control the hole dimensions.

[2] It is noted that the optical microscope was focused on the surface scratches as best as possible using the edge of the hole as a reference. However, in specimens, where the scratches had healed and the edges of the hole showed scale formation, the surface features and edge of the hole were not prominent, which made it difficult to focus. Also, light reflection from the bottom of the hole sometimes made it difficult to unambiguously establish whether the additive was healing the hole.

and extracting the QPA data. Therefore, the QPA data must be interpreted with some degree of caution. It is noted that the presence of free carbon can lead to a reaction with $CrSi_2$; otherwise, it has been demonstrated that $CrSi_2$ does not react with either SiC or Si_3N_4 (Ref. 27). Although the specimens appeared to be nearly fully consolidated in the microstructural observations, detailed void volume fraction measurements revealed that the specimens were fairly porous (Ref. 14). The measured volume fraction of the closed porosity were between 1.1 and 3.7%, while that of open porosity varied between 33.7 and 39.4%. The total porosity varied between 36.2 and 40.6%.

3.1 Isothermal Oxidation of Engineered Matrices

Figure 4 compares the isothermal oxidation behavior of $CrSi_2$-EM, CrMoSi-EM, $MoSi_2$-EM, $TiSi_2$-EM and WSi_2-EM at 1600 K, where the weight change, ΔW per unit area, A, is plotted against the isothermal oxidation time, t. The isothermal data reported for CVD SiC and Si_3N_4 at 1573 K are also shown for comparison (Ref. 28). In comparison to the oxidation behavior of SiC and Si_3N_4, the engineered matrices exhibits a large initial weight change in the first few hours presumably due to the faster growth rate of the metal oxides compared to SiO_2. However, as the more protective silica layer begins to form, the oxidation rate slows down in accordance with the parabolic oxidation kinetic law (Ref. 29). An examination of Figure 4 reveals that the initial oxidation rates for $TiSi_2$-EM and WSi_2-EM are higher than those for $CrSi_2$-EM, CrMoSi-EM and $MoSi_2$-EM but the magnitudes of specific weight gain, $\Delta W/A$, for these engineered matrices are similar $t \approx 100$ h. The isothermal oxidation behavior of the $MoSi_2$-EM specimen shows a continuously increasing specific weight change with increasing oxidation time presumably because the protective SiO_2 had not completely covered the sample. As a result, the $MoSi_2$-EM was not considered for further development. In addition, as discussed elsewhere (Ref. 14), the $MoSi_2$-EM thermal expansion specimen showed extensive circumferential cracks after thermal cycling.

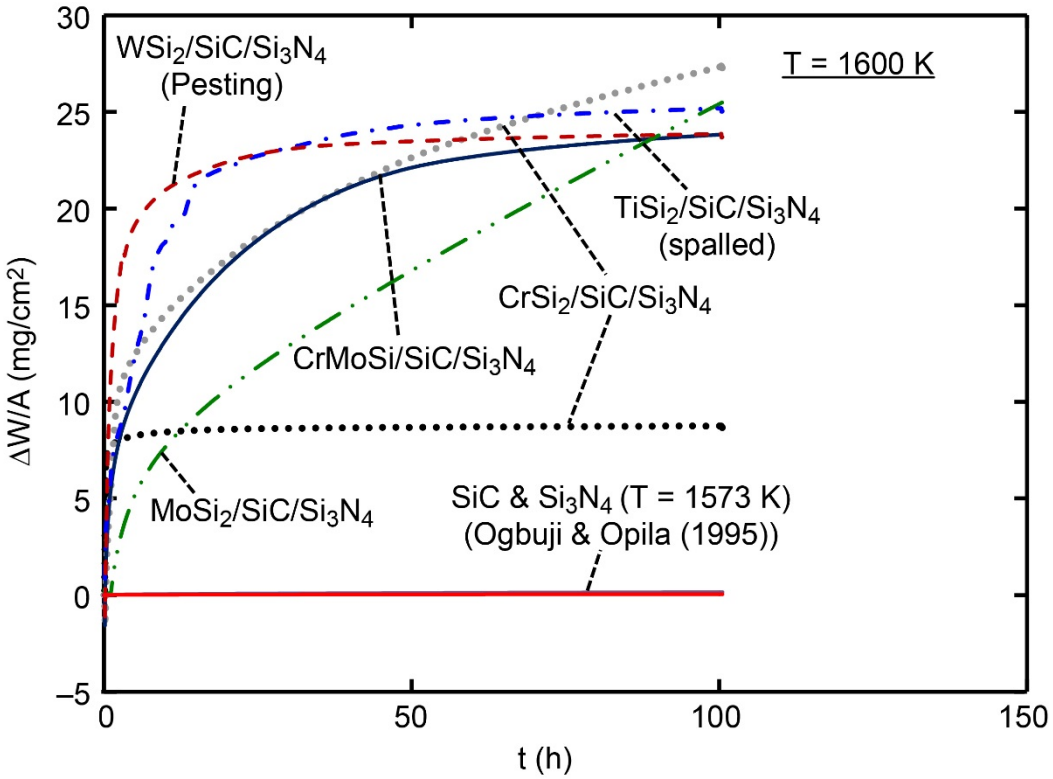

Figure 4.—Comparison of the isothermal oxidation behavior of several engineered matrices with those for CVD SiC (Ref. 28) and Si_3N_4 (Ref. 28) showing the change in the specific weight change with oxidation time.

Since the $TiSi_2$-EM spalled after 100 h, this matrix composition was eliminated from further consideration in the investigation. Although the WSi_2-EM did not show significant catastrophic oxidization (i.e., "pesting") or spalling during isothermal oxidation at 1600 K, it is noted that the WSi_2-EM bend specimens catastrophically oxidized and crumbled into powder during to heat-up to test temperature. This is probably due to the rapid oxidation of the W-rich particles observed in the hot-pressed microstructure (Ref. 14) leading to "pesting".

Curiously, the oxidation rates for the two $CrSi_2$-EM specimens were quite different, where one of the specimens exhibited relatively little specific weight gain after the initial oxidation while the other specimen continued to gain weight even after 100 h. This difference in behavior is attributed to an inhomogeneous distribution of the $CrSi_2$ particles. Similarly, the isothermal oxidation curve for CrMoSi-EM specimen shows an initial increase in the specific weight change with the formation of Cr_2O_3 before tending to flattening out as SiO_2 forms a protective layer. It is important to note that Cr_2O_3 forms a protective oxide scale for austenitic stainless steels and some nickel-base superalloys below 1000 °C, while SiO_2 is the protective oxide for SiC and Si_3N_4. Thus, $CrSi_2$-EM and CrMoSi-EM were chosen for further development since they are capable of forming both Cr_2O_3 and SiO_2 as protective oxides without any evidence of "pesting" or spalling. It is also important to note that the rapid formation of Cr_2O_3 in the initial stages of oxidation as evidenced in Figure 4 indicates that the presence of Cr in $CrSi_2$-EM and CrMoSi-EM is likely to getter any oxygen that may enter the matrix in a CMC through externally connected cracks. Thus, these chromium silicide EMs are likely to protect the oxidation of the BN coatings on the fibers.

3.2 Bend Properties of Engineered Matrices

As discussed in Section 1.0, one of the requirements of an effective EM is the ability to blunt cracks and prevent their propagation through the matrix. Once the crack propagation is prevented, the strength of the matrix, and correspondingly the CMC, is expected to increase. The important point to note is that developing local plasticity around the crack tip is imperative rather than increasing the "general plasticity"[3] of the matrix, since the latter approach is likely to decrease matrix strength at high temperatures, and that of the CMC, as it is likely to lead to significant matrix creep. Thus, a high concentration of homogeneously distributed ductile particles is expected to lead to "general plasticity" whereas a low concentration or a heterogeneously distribution of ductile particles is expected to result an increased tendency towards local plasticity of the matrix. Figure 5 shows the four-point bend stress, σ_B, versus bend strain, ε_B, plots for $CrSi_2$-EM at temperatures varying between room temperature and 1643 K[4]. A close examination of Figure 5 reveals that $CrSi_2$-EM is brittle below 898 K, and subsequently exhibits a low bend strength. However, the bend strength and bend plasticity increase significantly at 1173 and 1273 K presumably because the $CrSi_2$ particles exhibit limited ductility sufficient to blunt the crack tip. At 1377 and 1473 K, relatively large values of ε_B are observed with correspondingly lower magnitudes of σ_B that that observed at 1273 K. These observations are most likely due to an increase in the "general plasticity" of the matrix as the $CrSi_2$ particles become more ductile and they are homogenously distributed in the matrix.

[3] It is noted that the term "general plasticity", which is only relevant when describing metal plasticity, is used in this paper in an imprecise and qualitative manner to distinguish the toughness of these ceramic matrices.

[4] The legends identifying each curve in Figures 5 and 6 show three sets of digits. The first set refer to the hot-press run number, the second set the specimen number from a hot press run, and the third set refers to test temperature in K. For example, 625-3-RT in Figure 5 indicates that the hot-pressing batch was 625, and the third bend specimen machined from this batch was tested at room temperature.

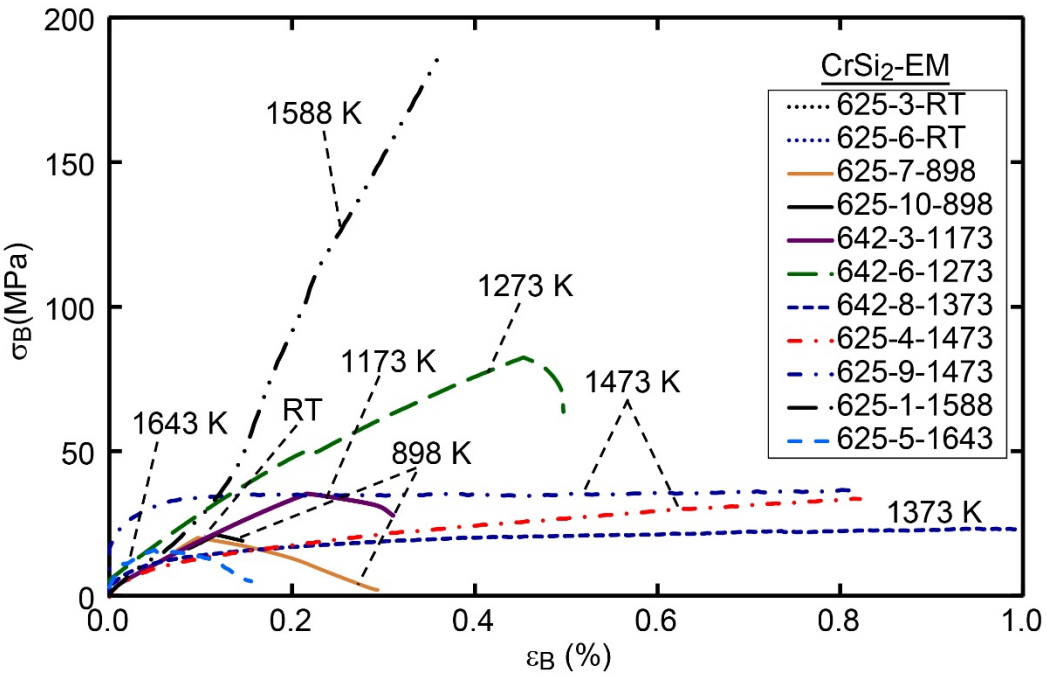

Figure 5.—Four-point bend stress-bend strain curves for $CrSi_2$-EM tested in air between room temperature (RT) and 1588 K showing that the bend strength increases with increasing temperature due to an increase in plasticity.

A basic premise in the current thesis requires the crack tip to meet a ductile silicide particle to blunt it and thereby increase matrix toughness. As indicated earlier, local plasticity at the crack tip is more desirable than "general plasticity" to enhance matrix strength. In both instances, it is necessary that the ductile silicide particles be homogenously distributed in the matrix. If the propagating crack fails to meet a ductile particle, the expected outcome is brittle behavior and low matrix strength. An examination of Figure 5 reveals that the observed σ_B-ε_B curves for the specimens tested at 1588 and 1643 K are inconsistent with the reported trend observed for the specimens tested between room temperature and 1473 K. These observations are attributed to an inhomogeneous distribution of the $CrSi_2$ particles leading to two possible outcomes depending on the path that the cracks follow as they propagate through the matrix. First, if the dominant propagating crack grows through $CrSi_2$ particle-rich regions, the local plasticity around the crack tip would blunt it thereby leading to an increase in the matrix strength. In this case, the overall bend strain would be expected to be lower than those for the specimens with a homogeneous distribution of $CrSi_2$. This appears to be the case with the specimen tested at 1588 K, where there is a considerable increase in the bend strength but with lower bend ductility than the specimens tested between 1273 and 1473 K. Second, if the dominant crack propagates through the predominantly brittle SiC-Si_3N_4 regions of the matrix instead of the $CrSi_2$ particle-segregated regions, the matrix is likely to be brittle. This appears to be the case for the specimen tested at 1643 K.

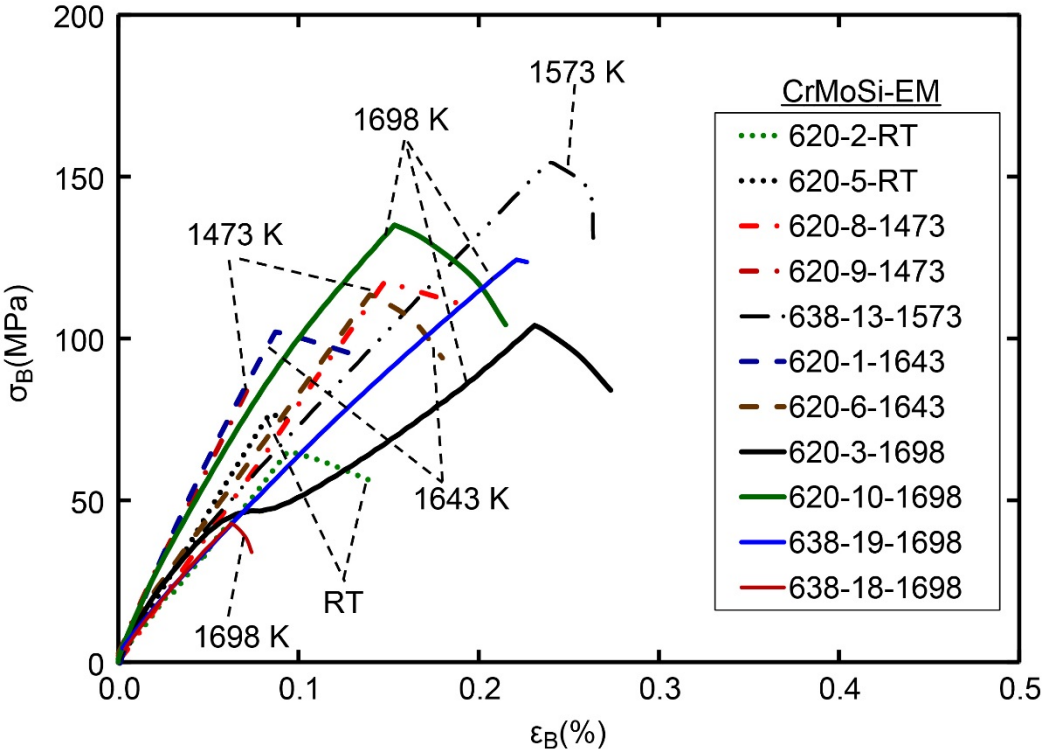

Figure 6.—Four-point bend stress-bend strain curves for CrMoSi-EM tested in air between room temperature (RT) and 1698 K showing that the bend strength increases with increasing temperature due to an increase in plasticity.

Figure 6 shows the four-point σ_B-ε_B curves for CrMoSi-EM between room temperature and 1698 K. The CrMoSi alloy is a high strength alloy with a compressive ductile-to-brittle transition temperature of about 1400 K (Refs. 21 and 22). Since the melting point of CrMoSi (Refs. 21 to 23) is much higher than that of $CrSi_2$, which is 1763 K (Ref. 30), the DBTT of CrMoSi is expected to be higher than that of $CrSi_2$ so that its brittleness extended to higher temperatures. Nevertheless, the σ_B-ε_B curves for CrMoSi-EM show a similar trend as the observations of $CrSi_2$-EM with increasing temperature. Once again, it is observed that CrMoSi-EM is brittle at room temperature but its bend strength and bend ductility increase with increasing temperature at and above 1473 K, where the CrMoSi particles begin to exhibit ductility (Refs. 21 and 22). However, batch-to-batch variations, as well as within batch disparities, are observed in the data thereby suggesting that the results are primarily sensitive to segregation of the matrix constituents although the role of other factors, such as machining defects, cannot be completely ruled out. Nevertheless, the basic premise underlying the design of an engineered matrix that ductile phase toughening at the operating temperatures sufficient to blunt crack tips would result in an increase matrix strength is proven by the present observations. Additional investigations are required to improve the homogenous distribution of the matrix constituents so as to reduce scatter in the data and improve reproducibility.

3.3 Self-Healing Studies

3.3.1 Effect of Additives

An initial assessment of additives on the self-healing characteristics of engineered matrices revealed that they were effective in healing scratches and closing a ~1 mm diameter hole to various degrees. After oxidation at 1600 K for 24 h, CrMoSi-SiC specimen without any additives showed no significant healing of the scratches and the hole (Fig. 7(a)). However, adding 1(wt.%) CrB_2 had a significant effect on healing the scratches, but no significant oxide scale was evident at the edges of the hole (Fig. 7(b)). The addition of 5(wt.%)CrB_2 healed the scratches on the specimen surface while allowing an oxide scale to form at the edges of the hole (Fig. 7(c))[5]. Continued oxidation at 1700 K for a cumulative oxidation time of 100 h showed that the hole on the exposed top face (Figs. 8(a) and (c)) had significantly closed relative to that on the rear face (Figs. 8(b) and (d)). In this case, significant scratch healing and hole closure are observed. The presence of 1(wt.%)Ge in the CrMoSi alloy as a solid solution was not as effective in healing the scratches and closing the hole unlike the addition of 1(wt.%) $CrB_2$to the matrix (Fig. 7(d)). The amount of Y in the CrMoSi alloy was 0.1 wt.%, which was insufficient to significantly heal the scratches (Fig. 7(e)). Figure 7(f) shows the effectiveness of 1(wt.%)$ZrSiO_4$ in healing scratches (Fig. 7(f)). An oxide scale was observed at the edge of the hole. The addition of 5(wt.%) $ZrSiO_4$ was quite effective in healing the scratches, and although the edge of the hole showed a thick oxide scale (Fig. 7(g)).

Figures 9(a) to 12(a) show scanning electron images while Figures 9(b) to 12(b) show the corresponding backscattered images of the holes. Several small white particles were observed at the bottom of the holes (Figs. 9(b), 10(b), 12(b), and 12(d)) and on the specimen surfaces (Figs. 9(c), 10(c), 11(c), and 12(f)). The EDS spectra from these particles showed O, Si and Zr peaks, which suggested that they were probably zirconium silicate. Since zirconium silicate was intentionally added as a self-healing additive in two compositions, it was concluded that these white particles were furnace contaminants. The presence of these particles had no significant effect on the nature of the composition and morphology of the oxide scale. Energy dispersive spectra of the oxide scales formed on these specimens after oxidation at 1700 K for a cumulative oxidation time of 100 h revealed O and Si peaks, and it was concluded that they were silica (Figs. 9(d), 10(c), 11(c), and 12(e)).

The morphology of the scale was influenced by the additive. Without any additives, the morphology of the scale was granular (Fig. 9(c)). Silica globules were observed with the addition of 5(wt.%) CrB_2 (Fig. 10(c)). In contrast, Ge addition resulted in a “mud flat” scale morphology thereby suggesting a low viscosity scale, which would be advantageous in filling cracks (Fig. 11(d)). The effect of Y on the scale was similar to that shown in Figure 9 but with more rounded and fused features (Figs. 12(d) and (f)). The specimen with $ZrSiO_4$ resulted in catastrophic oxidation at 1700 K.

Similarly, 5(wt.%) CrB_2 and 5(wt.%) $ZrSiO_4$ additions to 20(wt.%) $CrSi_2$-75%SiC were effective in healing the scratches (Figs. 13(a) to (d)). There appeared to be a partial closing of the ~1 mm diameter hole, where the scale for the specimen with $ZrSiO_4$ was brittle, although $ZrSiO_4$ was more effective (Fig. 13(d)) than CrB_2 (Fig. 13(c)) in self-healing the damage. The relative change in the hole dimensions, $\Delta d/d_0 = (d_f-d_0)/d_0$, where d_f and d_0 are the final and initial diameters of the hole, relatively, significantly decreased with the addition of 5(wt.%) of either CrB_2 or $ZrSiO_4$ (Figs. 14(a) and (b)). For example, the hole dimensions closed by about 60% for CrMoSi/SiC oxidized at 1700 K for 100 h. However, specimens with $ZrSiO_4$ generally suffered catastrophic oxidation and the specimens fell apart.

[5] It was difficult to focus on this specimen surface due to the absence of any distinct features.

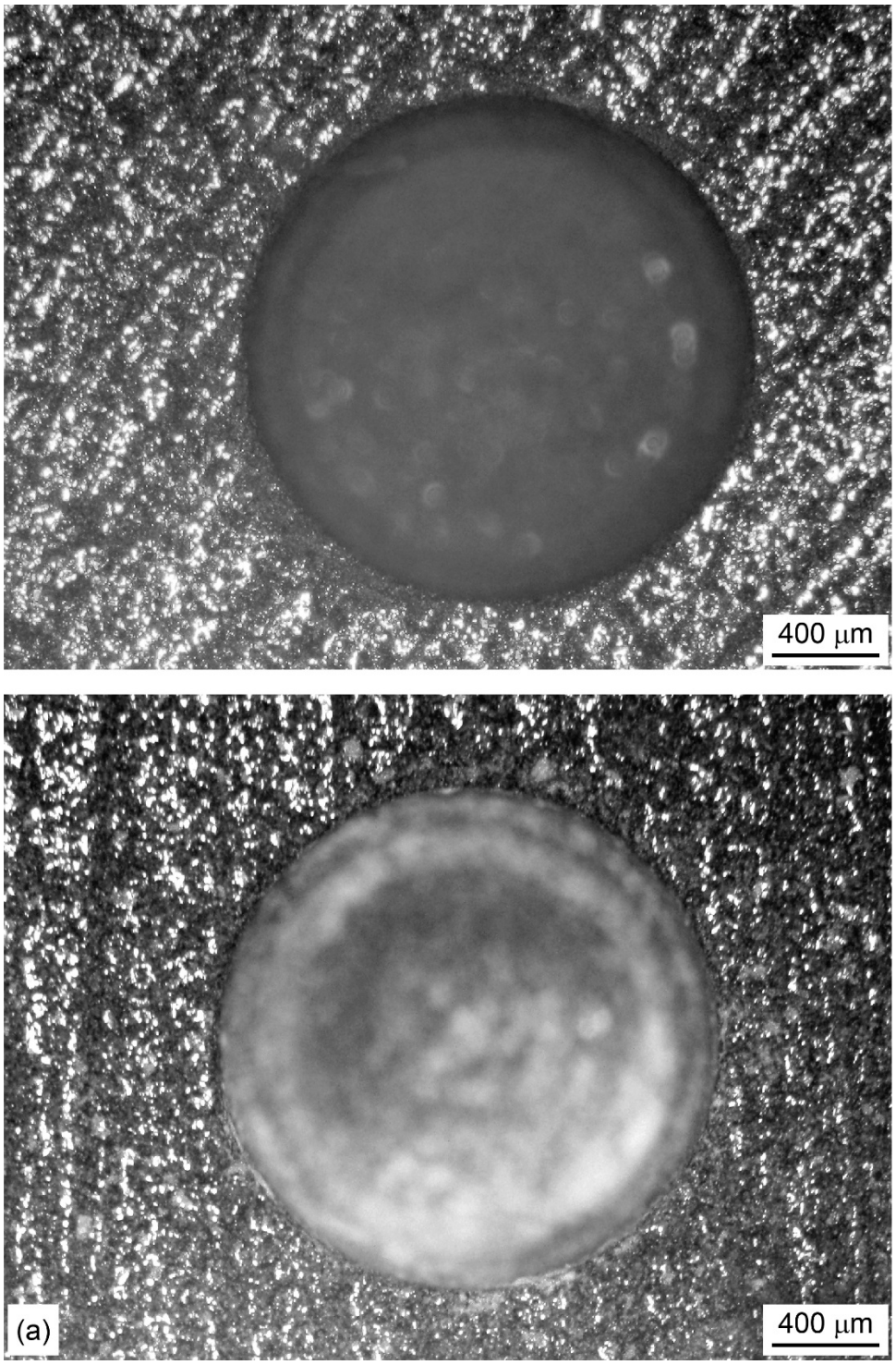

Figure 7.—Comparison of the effectiveness of additives on the self-healing of scratches and a 1 mm diameter hole before (top micrographs) and after (bottom micrographs) oxidation at 1600 K for 24 h. (a) 20(wt.%)CrMoSi-80%SiC; (b) 20(wt.%)CrMoSi-79%SiC-1%CrB_2; (c) 20(wt.%)CrMoSi-75%SiC-5%CrB_2; (d) 20(wt.%)CrMoSiGe-80%SiC; (e) 20(wt.%) CrMoSiY-80%SiC; (f) 20(wt.%)CrMoSi-79%SiC-1%$ZrSiO_4$ and (g) 20(wt.%)CrMoSi-75%SiC-5%$ZrSiO_4$.

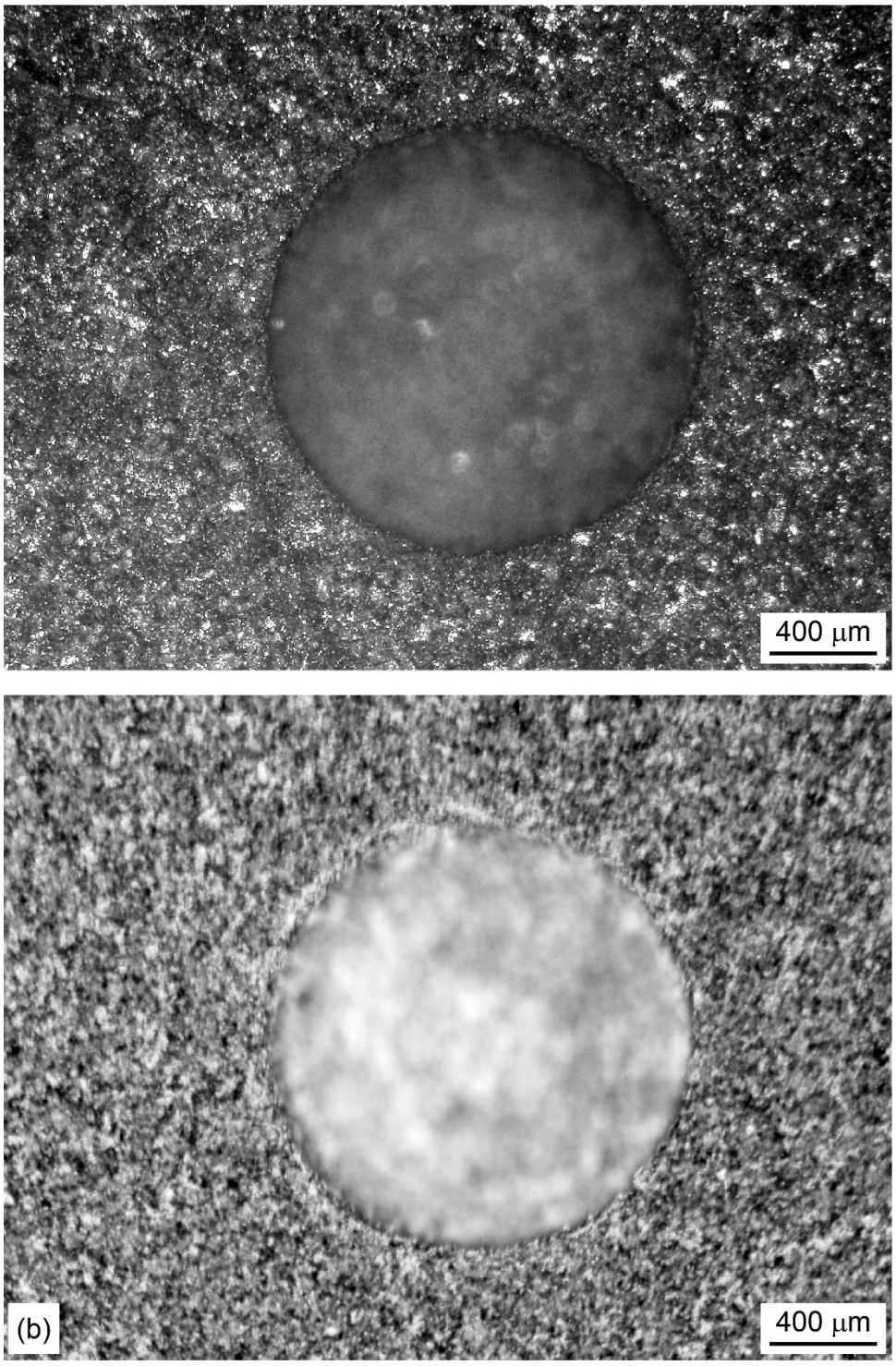

Figure 7.—Continued.

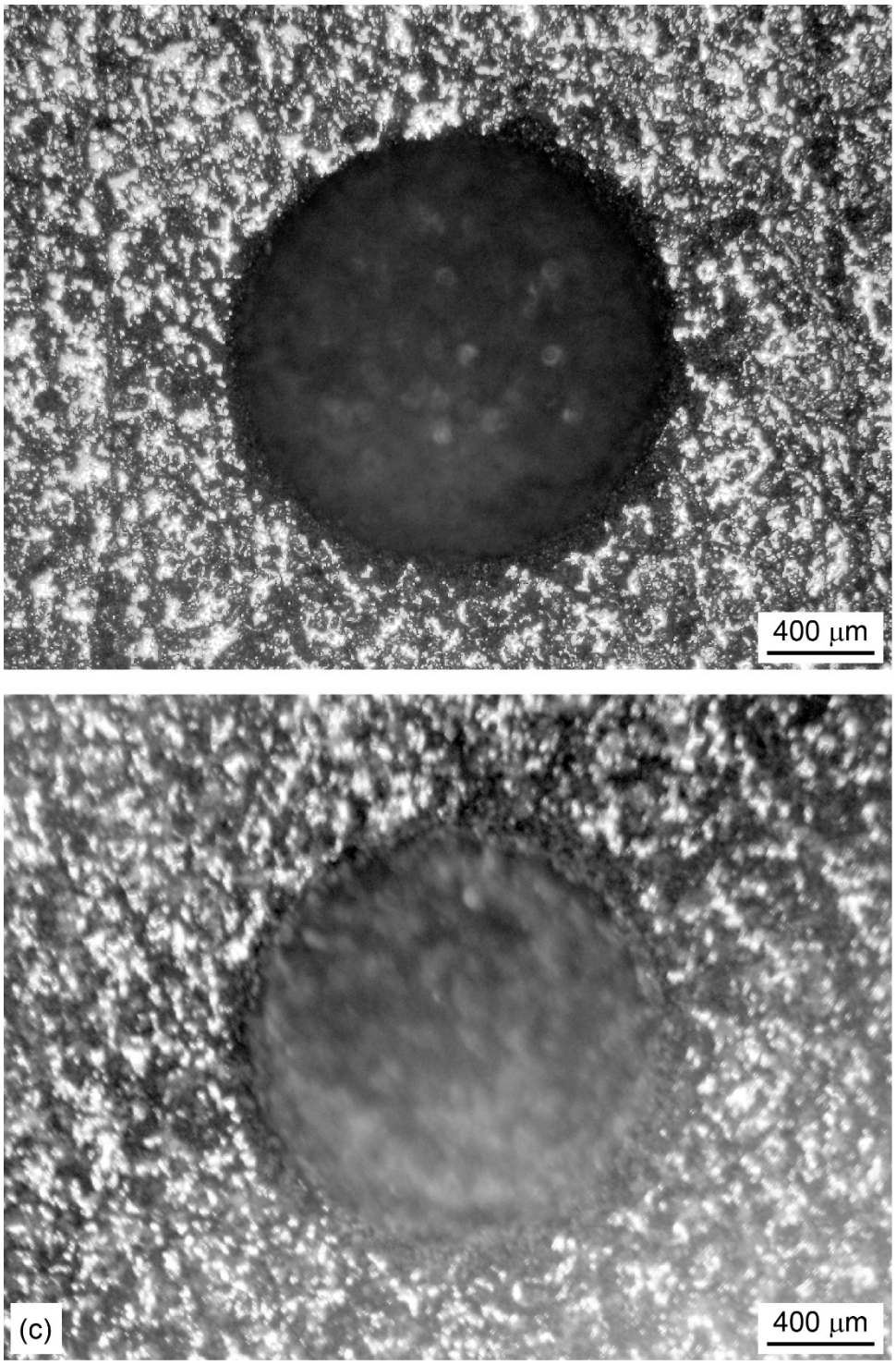

Figure 7.—Continued.

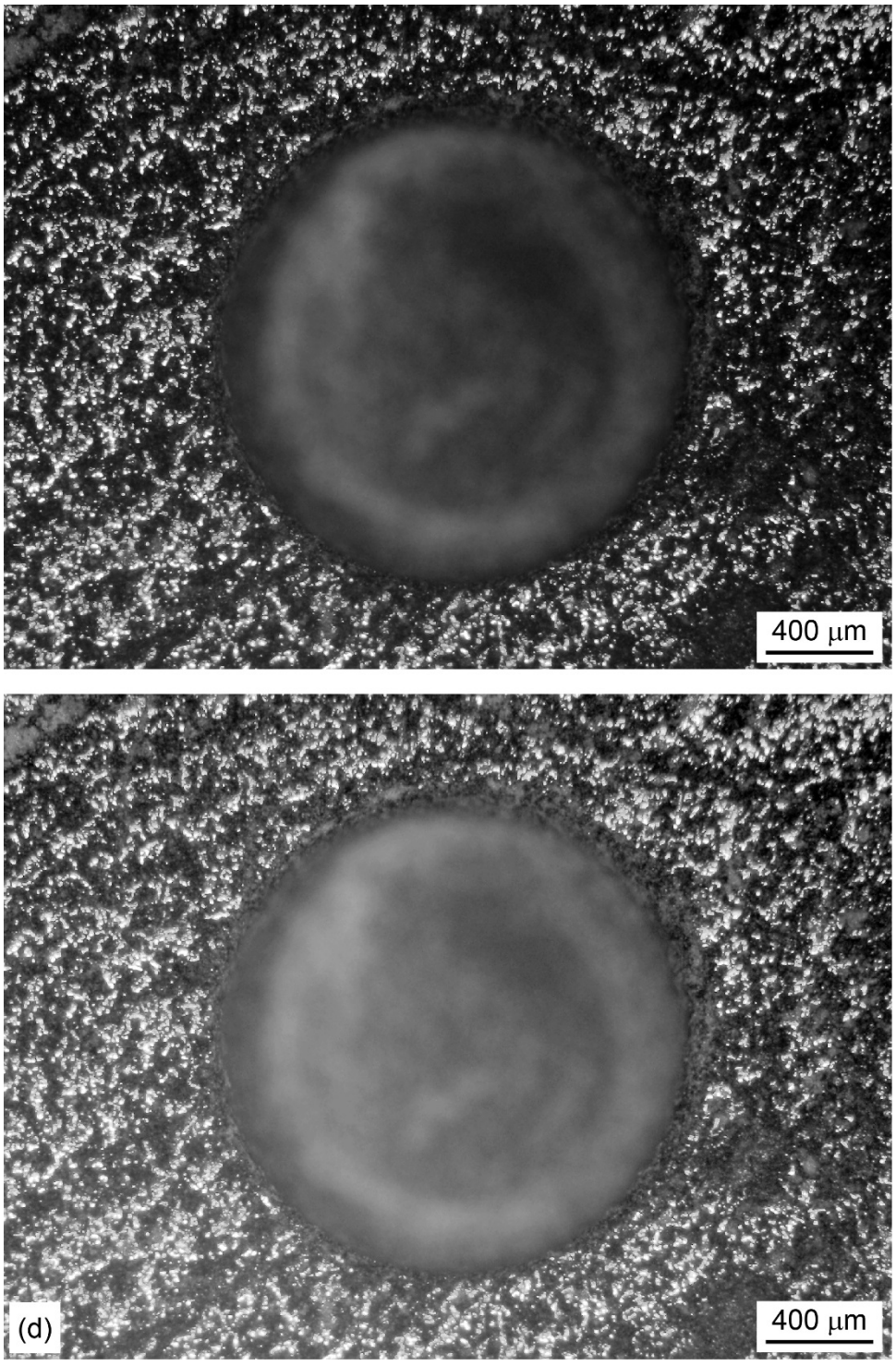

Figure 7.—Continued.

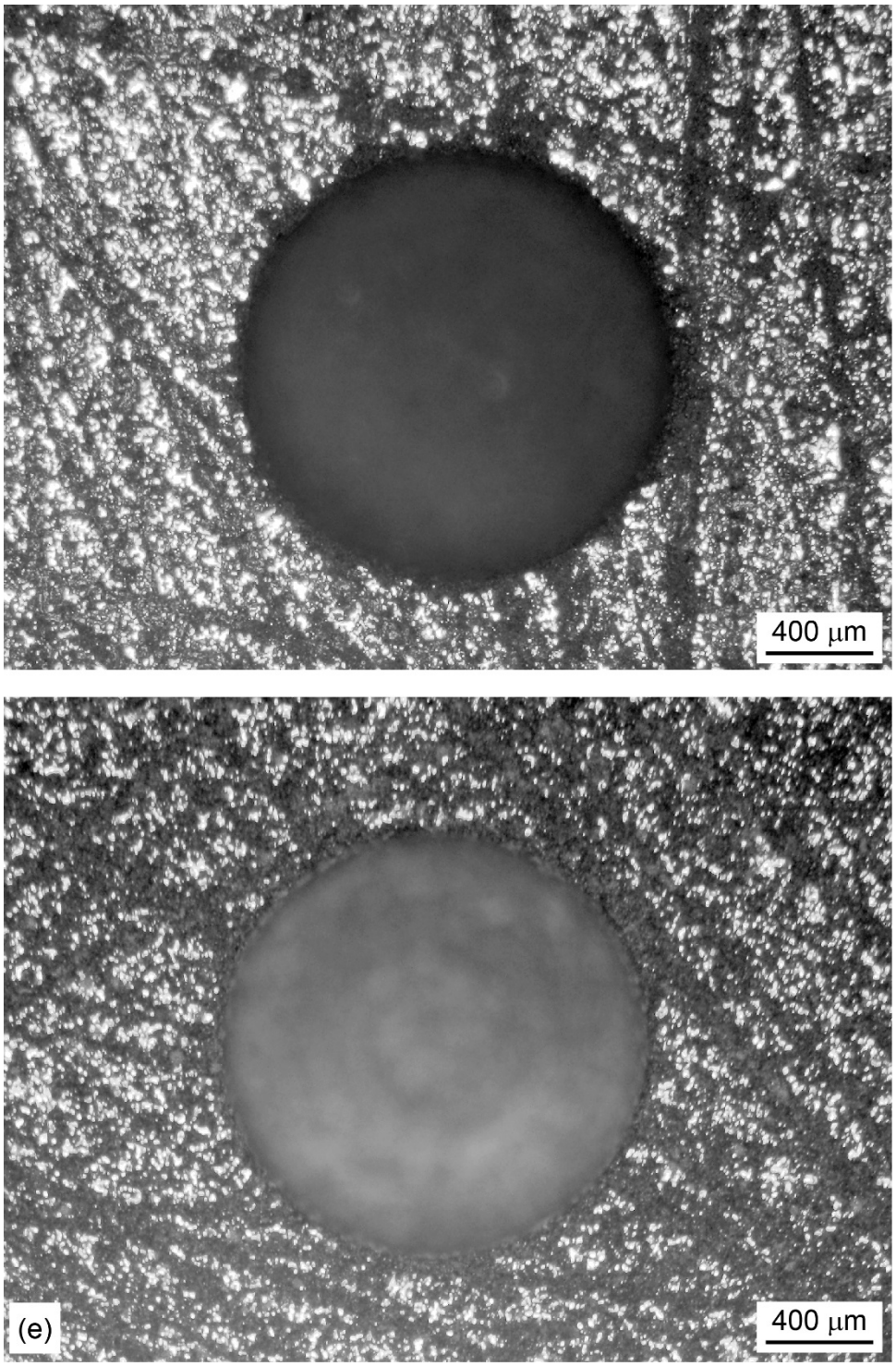

Figure 7.—Continued.

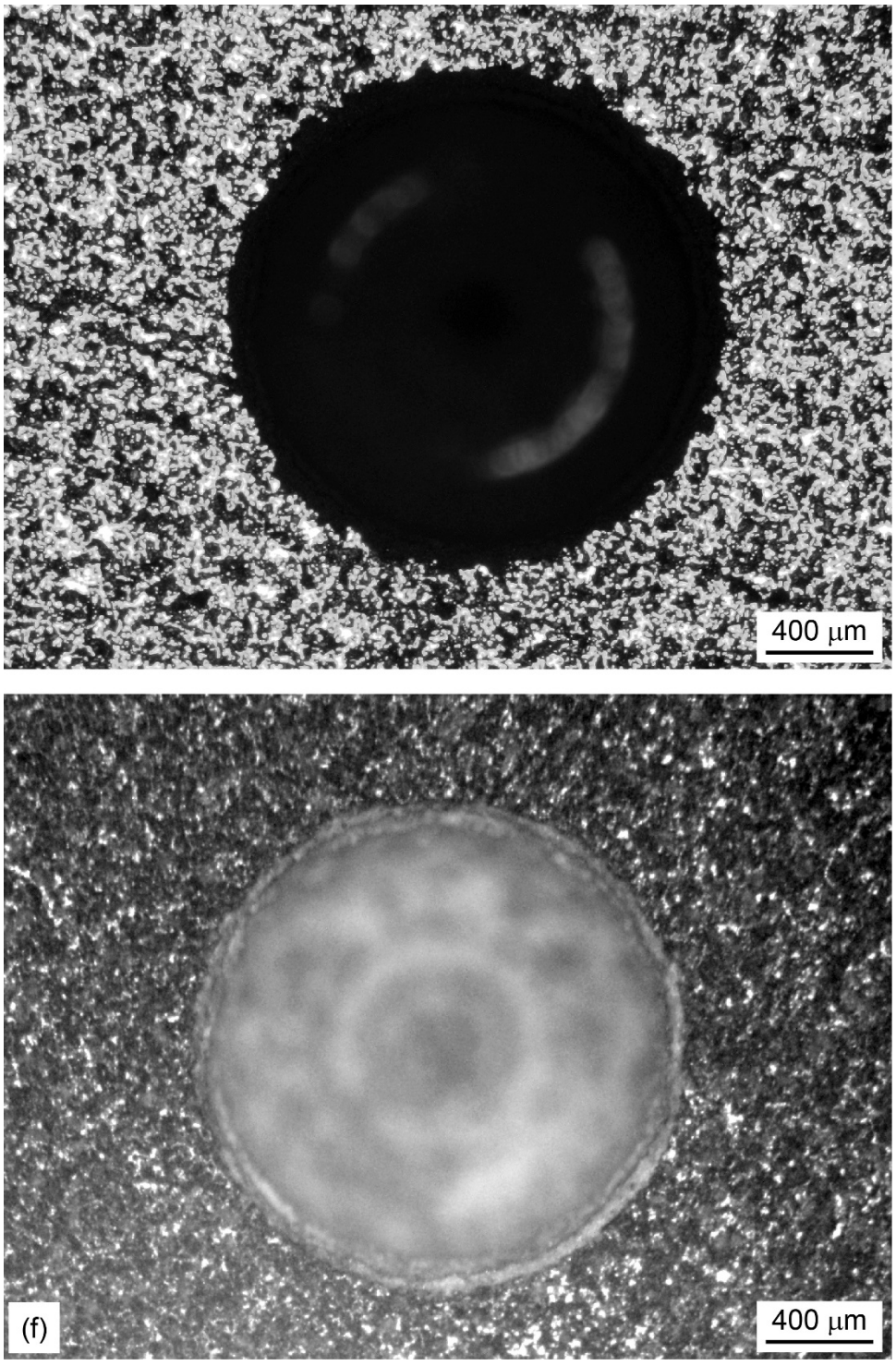

Figure 7.—Continued.

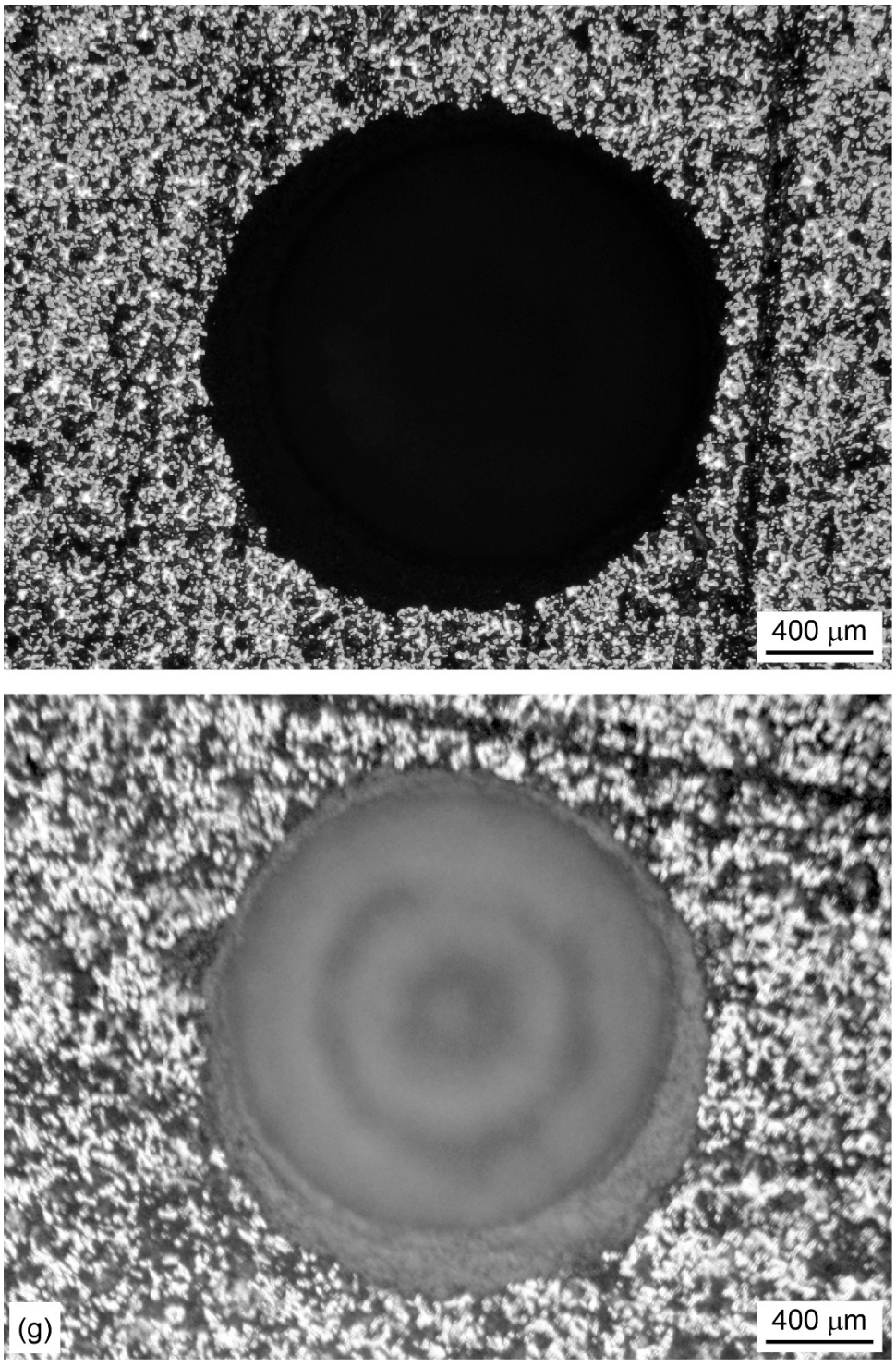

Figure 7.—Concluded.

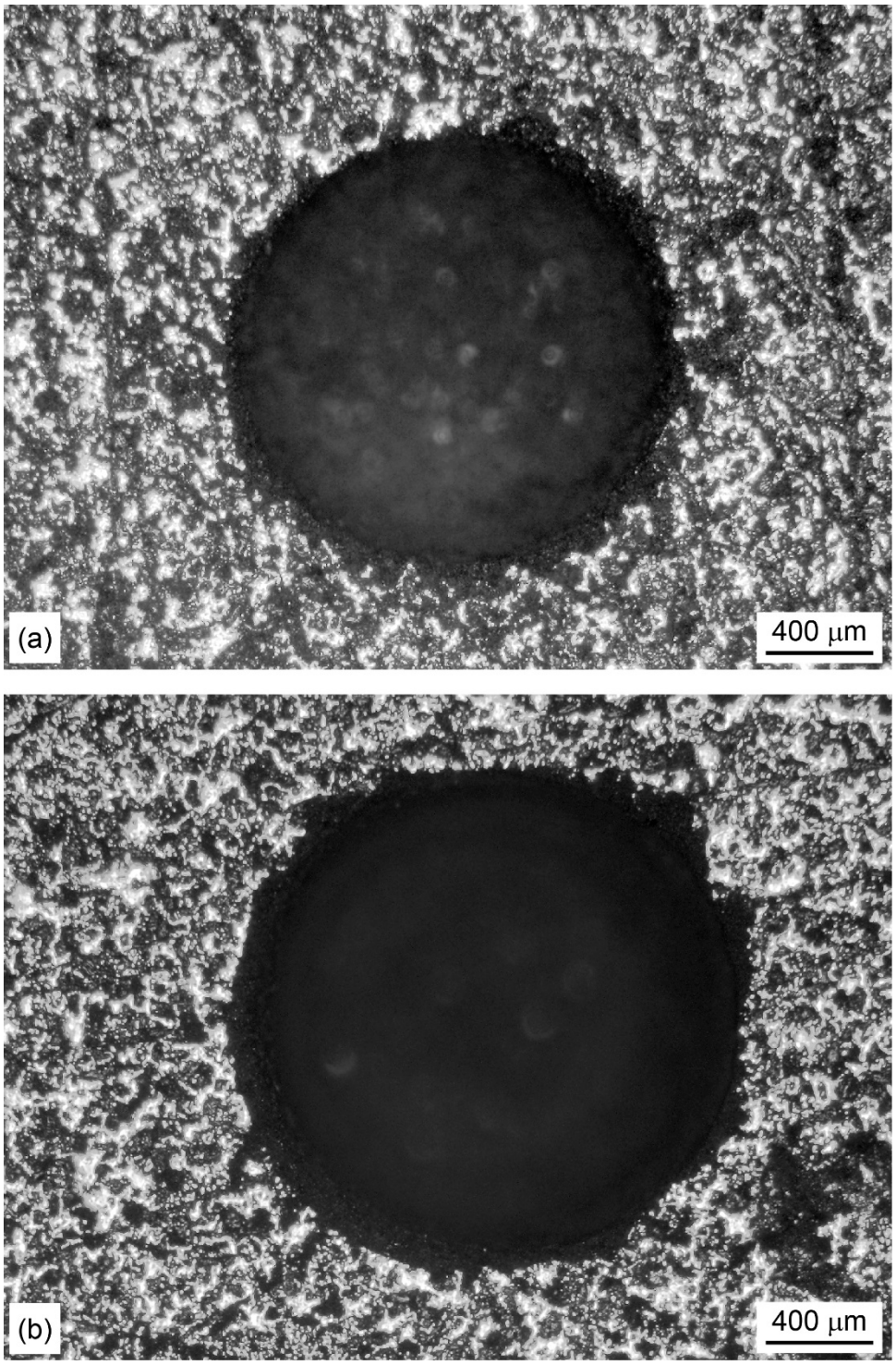

Figure 8.—Optical macrographs showing (a) and (c) the top face exposed to air and (b) and (d) the rear face on the tray bottom showing the extent of hole closure after oxidation of a 20%CrMoSi-75%SiC-5%CrB_2 at 1700 K for 100 h. Views of the holes (a) and (b) before oxidation; and (c) and (d) after oxidation.

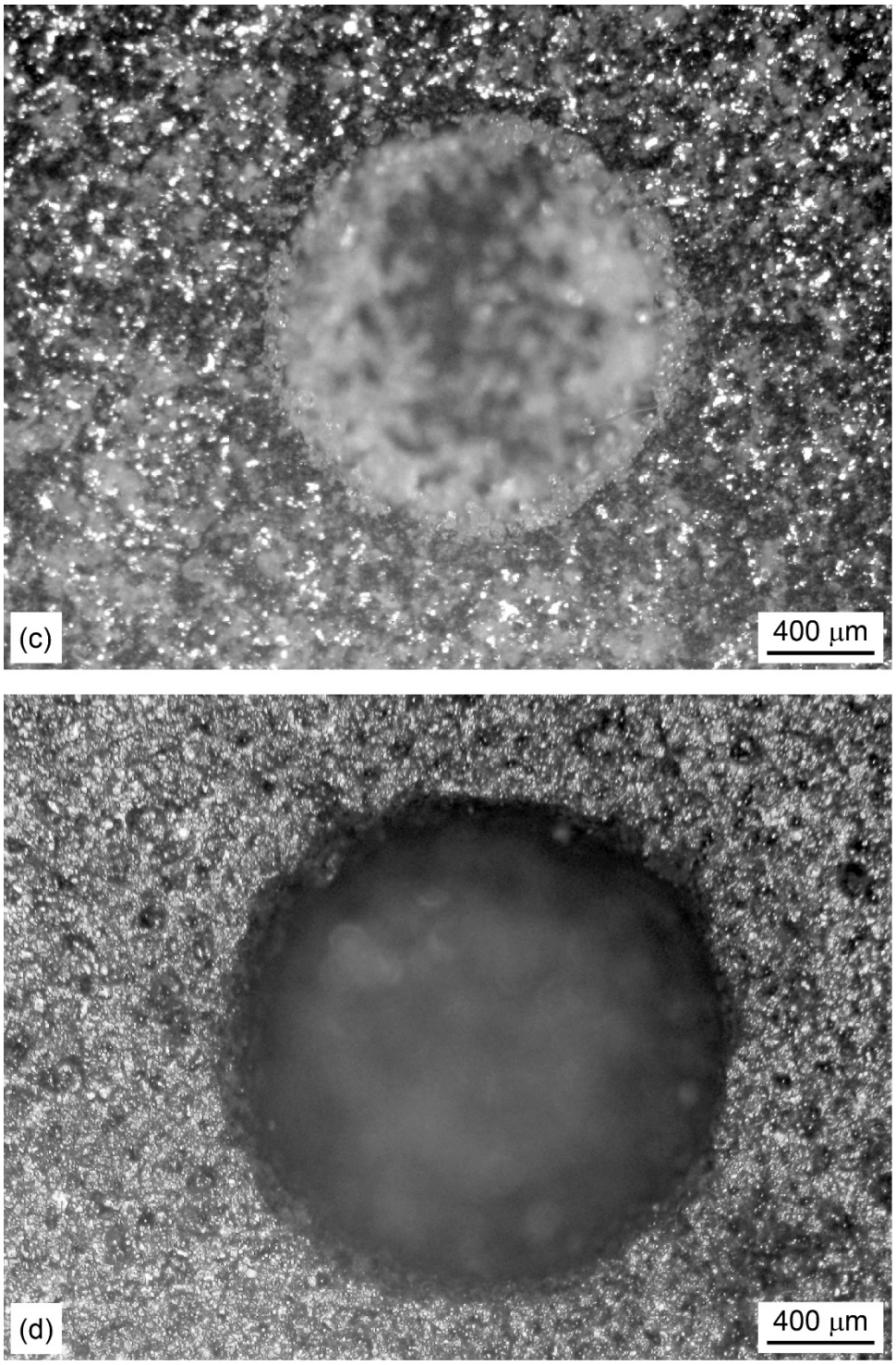

Figure 8.—Concluded.

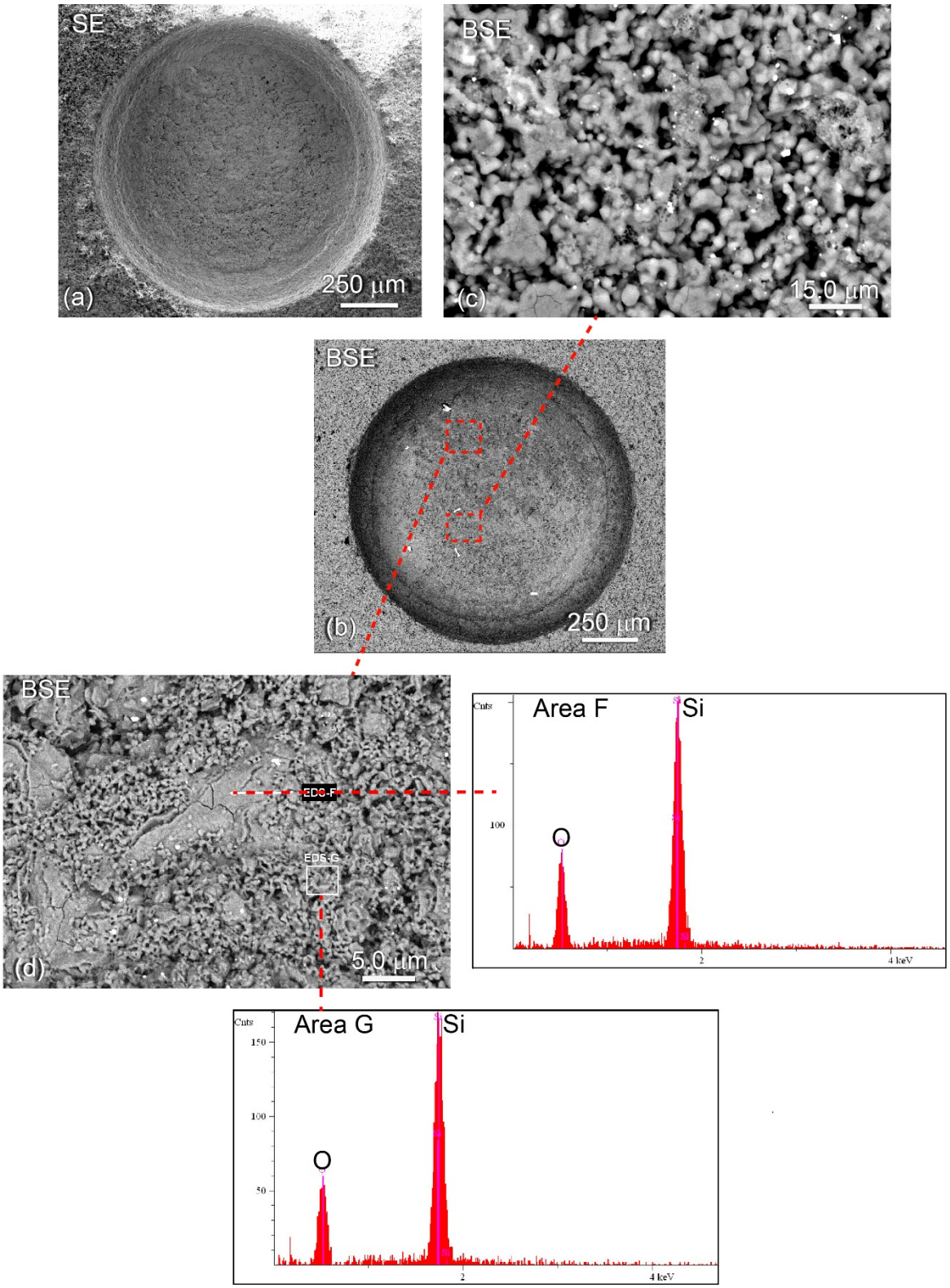

Figure 9.—Microstructures of 20(wt.%)CrMoSi-80%SiC after oxidation at 1700 K for a cumulative oxidation time of 100 h. Low magnification (a) scanning electron and (b) back-scattered electron images of the hole; (c) untilted high magnification BSE image of the bottom surface of the hole; and (d) a BSE image of a region from the bottom surface of the hole showing areas F and G from which energy dispersive spectra of the silica scale were obtained.

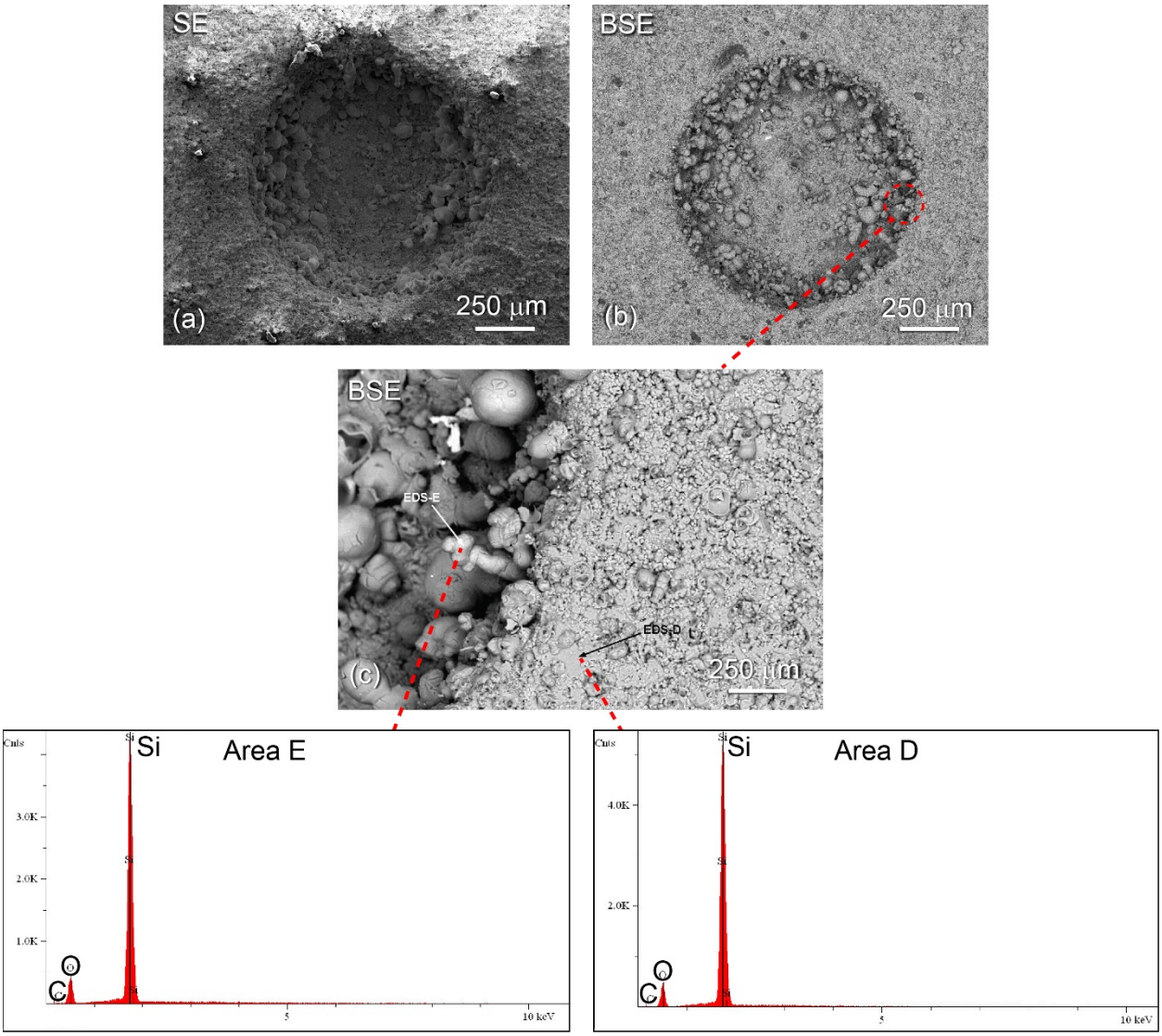

Figure 10.—Microstructures of 20%CrMoSi-75%SiC-5%CrB_2 after oxidation at 1700 K for a cumulative oxidation time of 100 h. Low magnification (a) scanning electron and (b) back-scattered electron images of the hole; and (c) untilted high magnification BSE image of a region of the specimen showing the locations of area E at the edge of the hole and area D on the surface of the specimen corresponding to the energy dispersive spectra of the silica scale.

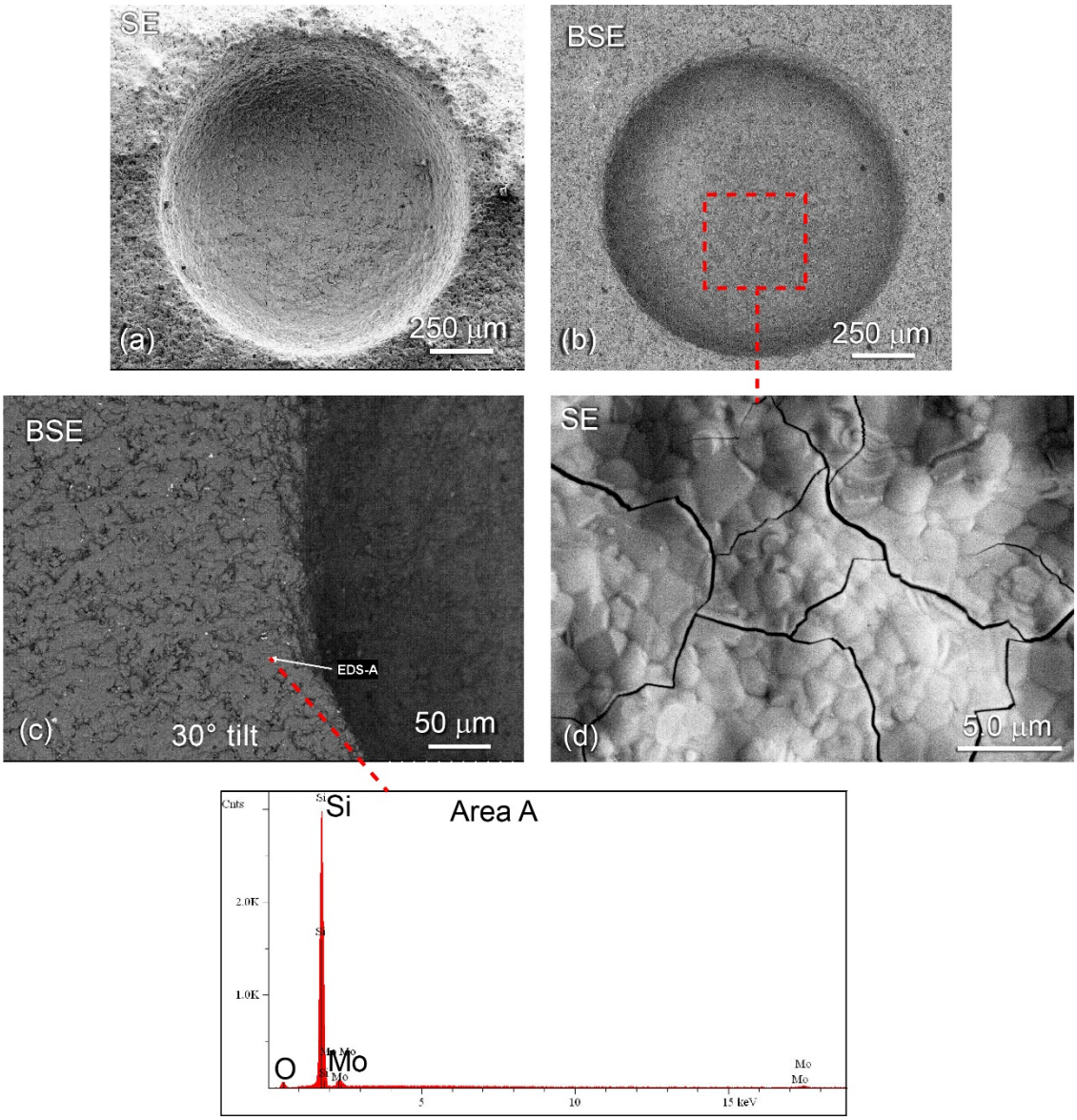

Figure 11.—Microstructures of 20%CrMoSiGe-80%SiC after oxidation at 1700 K for a cumulative oxidation time of 100 h. Low magnification (a) scanning electron and (b) back-scattered electron images of the hole; (c) 30° tilted high magnification BSE image of area A of the specimen surface close to the edge of the hole corresponding to the energy dispersive spectra of the silica scale; and (d) untilted high magnification BSE image of the bottom of the hole showing a “mud flat” morphology of the scale.

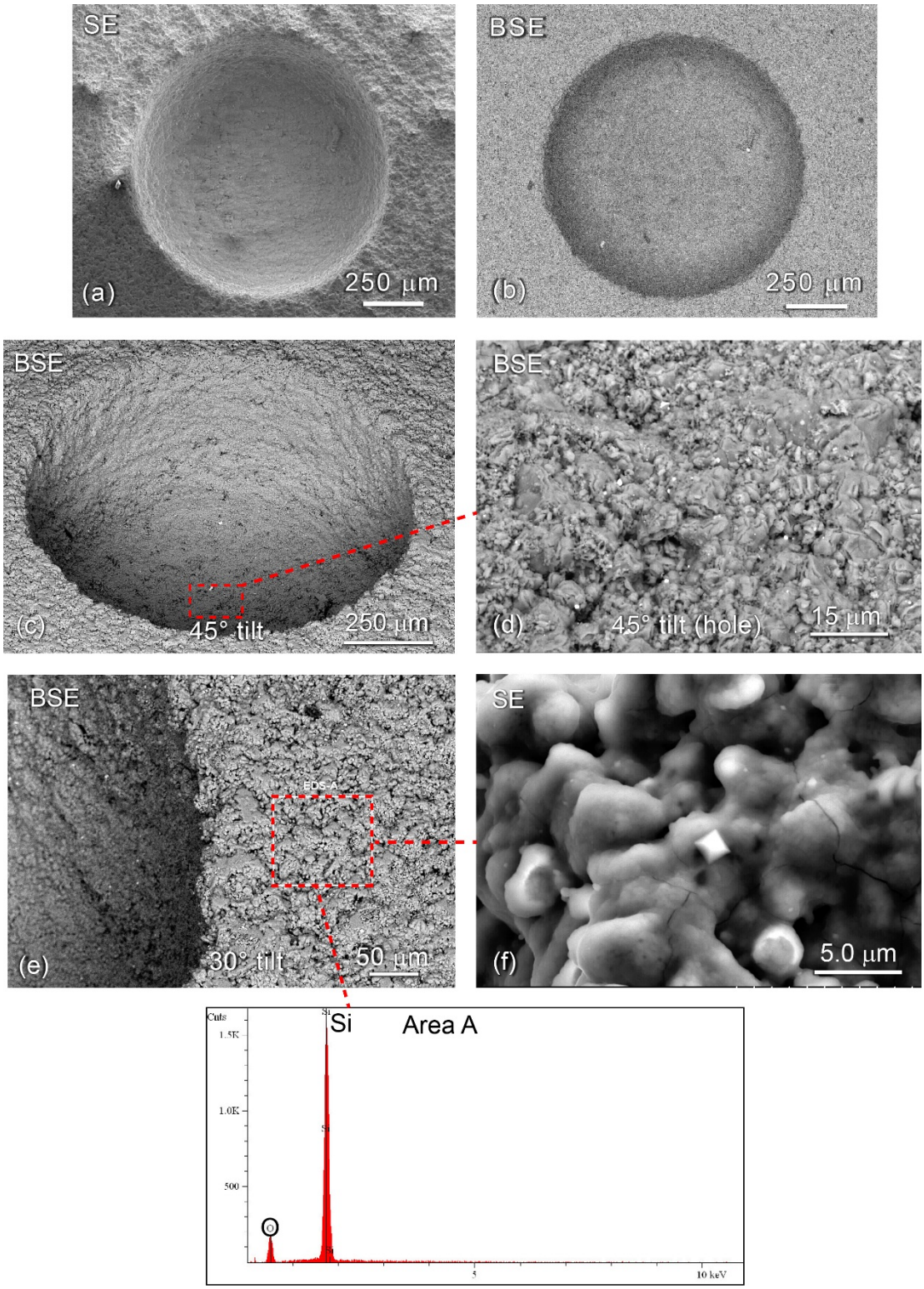

Figure 12.—Microstructures of 20%CrMoSiY-80%SiC after oxidation at 1700 K for a cumulative oxidation time of 100 h. Low magnification (a) scanning electron and (b) back-scattered electron images of the hole; (c) 45° tilted low magnification BSE image of a region of the specimen showing the edge of the hole and the surface; (d) high magnification BSE image of the area shown in (c); (e) 30° tilted BSE image of the specimen surface indicating the area corresponding to the energy dispersive spectra of the silica scale; and (f) high magnification BSE image of the area shown in (e).

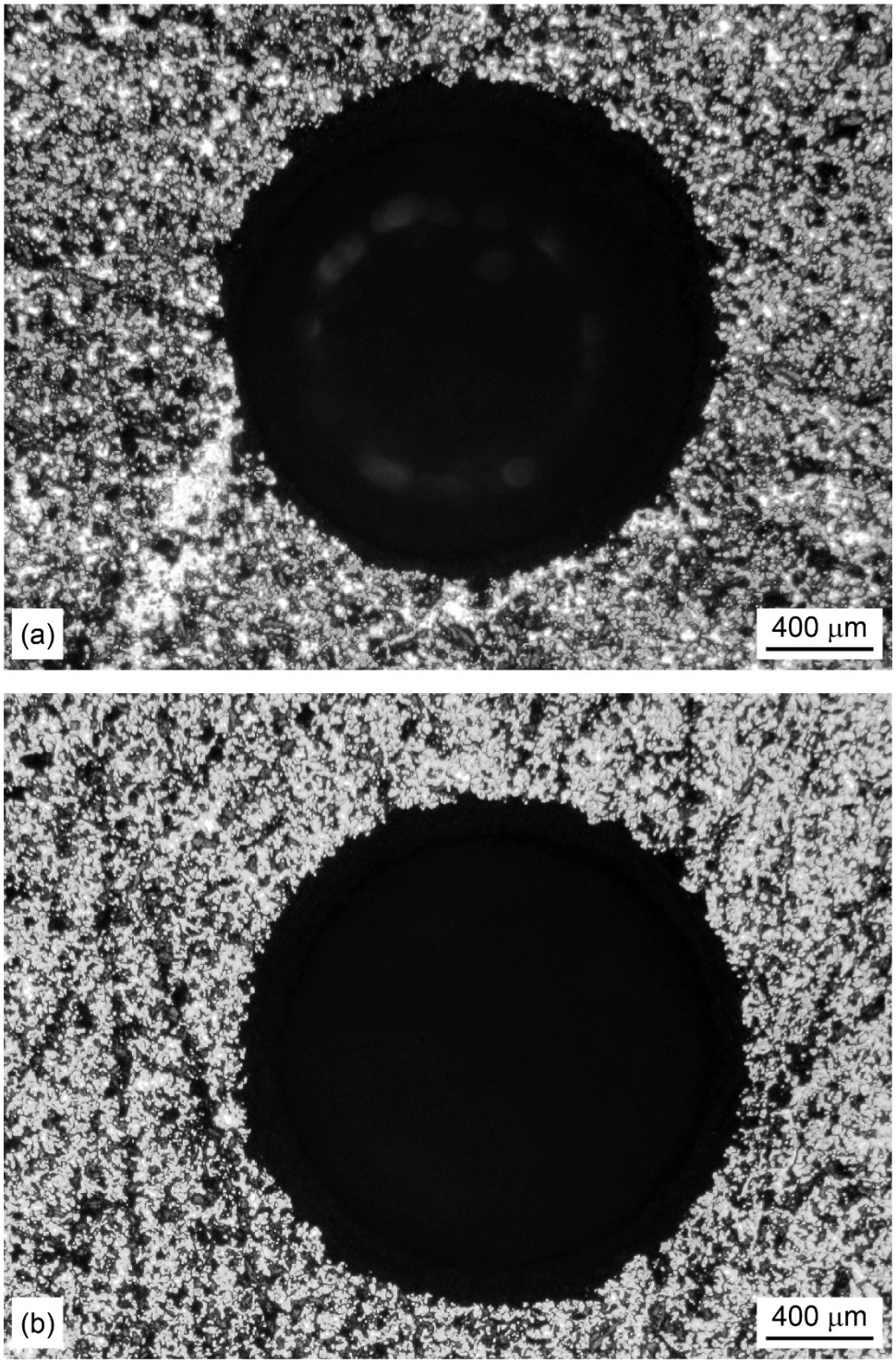

Figure 13.—Optical macrographs comparing the effectiveness of 5(wt.%)CrB_2 and 5(wt.%)$ZrSiO_4$ additives to the $CrSi_2$-SiC EM on the healing of scratches and the closure of a~1 mm diameter hole (a) and (b) before and (c) and (d) after oxidation at 1600 K for 24 h. (a) and (c) 20(wt.%)$CrSi_2$-75%SiC-5%CrB_2; (b) and (d) 20(wt.%)$CrSi_2$-75%SiC-5%$ZrSiO_4$.

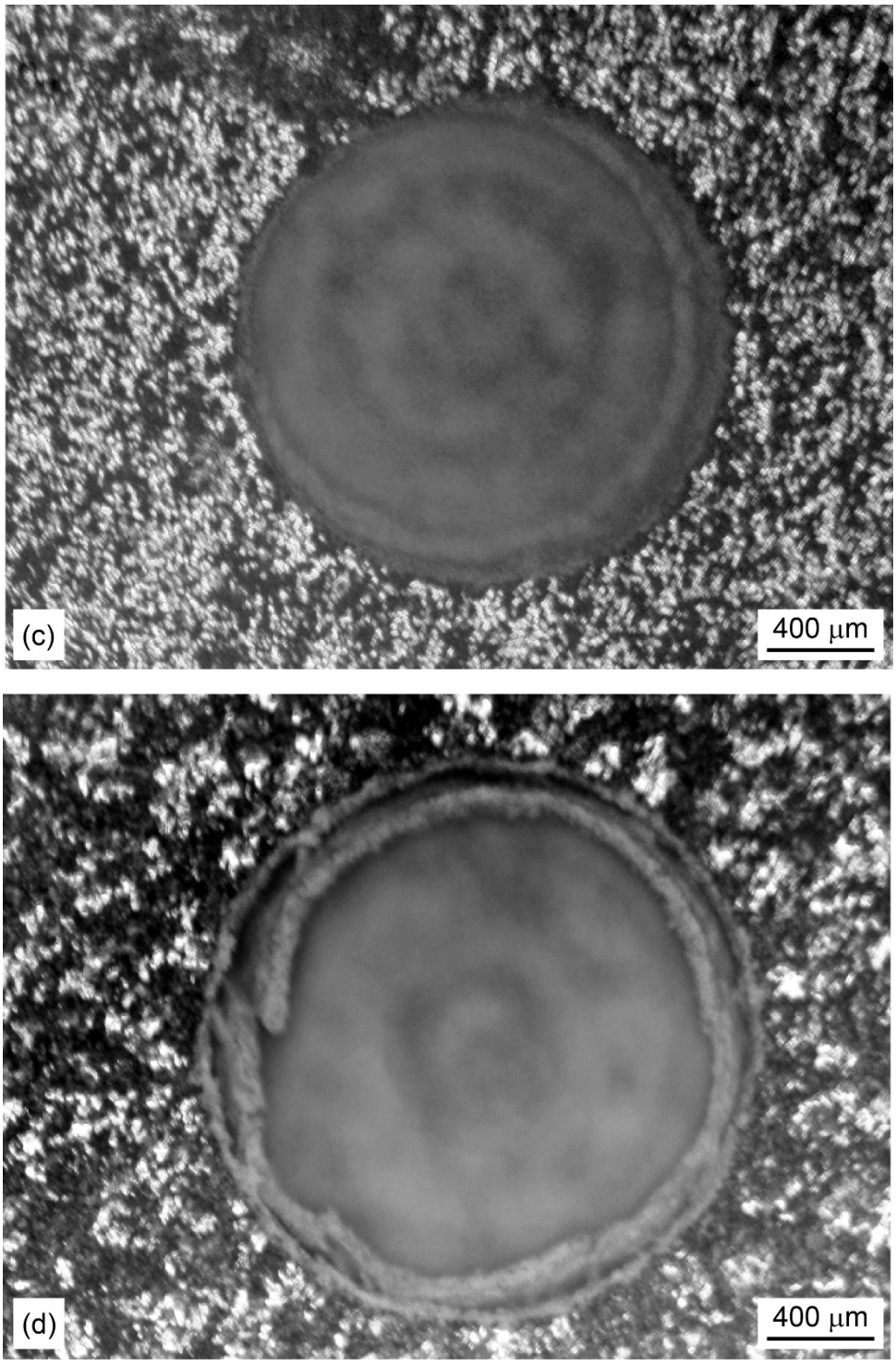

Figure 13.—Concluded.

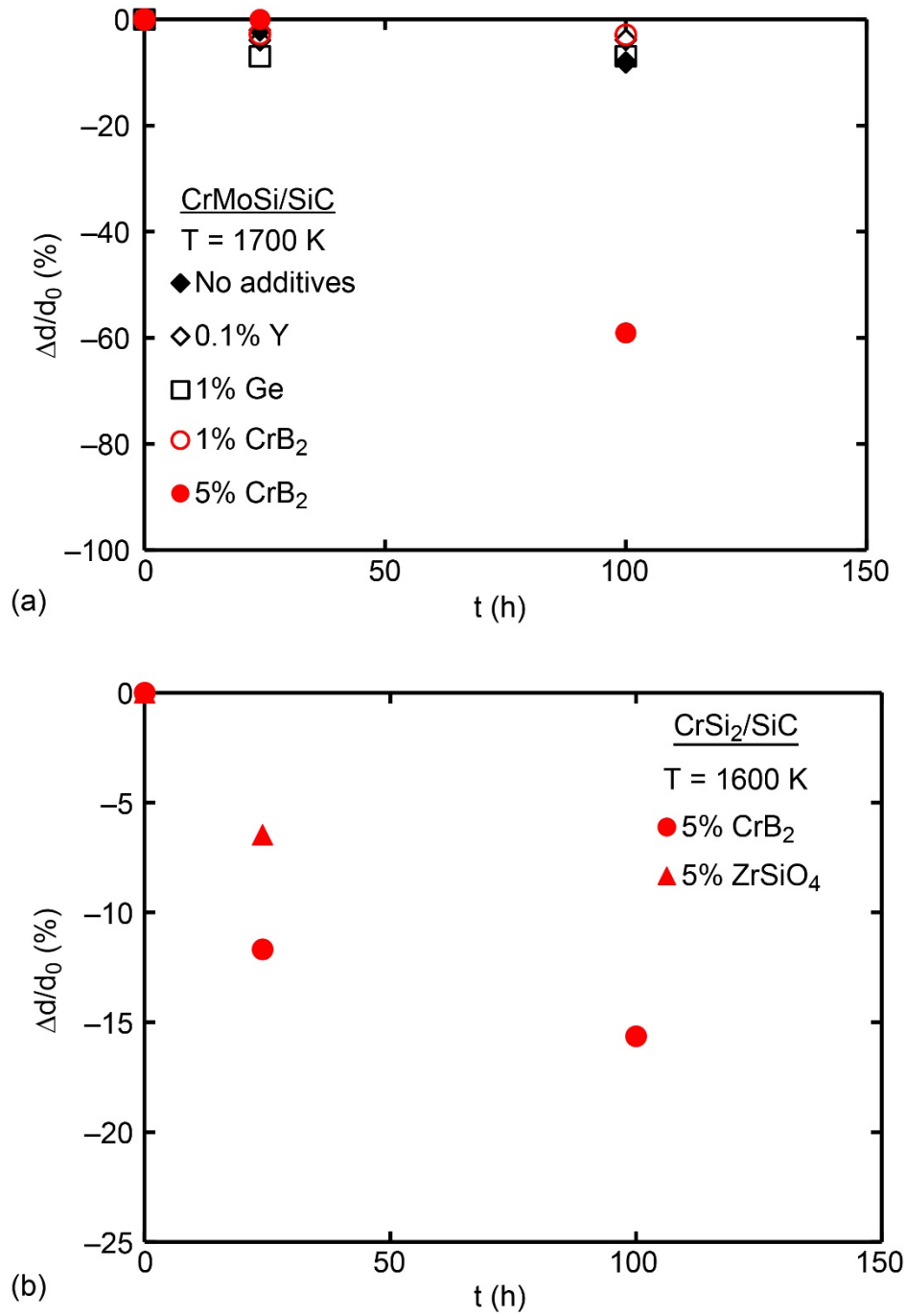

Figure 14.—Relative change in the hole dimensions versus oxidation time. (a) CrMoSi/SiC oxidized at 1700 K; (b) $CrSi_2$/SiC oxidized at 1600 K.

4.0 Summary and Conclusions

The design of an engineered matrix for an E-CMC must satisfy certain criteria, which are discussed in the present paper. Chief among them is that the thermal expansion of these engineered matrices should be close to that of the SiC_f reinforcing fibers. In an earlier paper (Ref. 14), it was proposed and demonstrated that the constituents of several silicide-based engineered matrices could be formulated using a rule of mixtures approach to ensure that their thermal expansions were relatively close to that of SiC. The present paper discusses the isothermal oxidation properties of 10(vol.%)$CrSi_2$-70%SiC-20%Si_3N_4 ($CrSi_2$-EM), 10(vol.%)CrMoSi-60%SiC-20%Si_3N_4 (CrMoSi-EM), 10(vol.%)$MoSi_2$-70%SiC-20%Si_3N_4 ($MoSi_2$-EM), 10(vol.%)$TiSi_2$-70%SiC-20%Si_3N_4 ($TiSi_2$-EM) and 10(vol.%)WSi_2-70%SiC-20%Si_3N_4 (WSi_2-EM) at 1600 K. In comparison to the isothermal oxidation behavior of CVD SiC (Ref. 28) and Si_3N_4 at 1573 K (Ref. 28), the engineered matrices exhibited a large initial weight change presumably due to the rapid formation of the metal oxides before generally leveling off as the protective SiO_2 scale begins to form. Based on the comparative isothermal oxidation behavior of several silicide-based EMs, only the $CrSi_2$-EM and the CrMoSi-EM compositions were downselected for further development since the other engineered matrices exhibited either "pesting" or the oxide layer spalled. Since the initial oxidation rates of these two chromium silicide-EMs were significantly higher than CVD SiC (Ref. 28) and Si_3N_4 (Ref. 28), the presence of Cr is expected to getter any oxygen ingress into the matrix through surface-connected cracks in an E-CMC thereby potentially protecting the BN coating on the SiC_f fibers. Four-point bend tests conducted on these two engineered matrix compositions demonstrated that the bend strength and bend strain generally increased with increasing temperature above the ductile-to brittle transition temperature of either the $CrSi_2$ or the CrMoSi particles. This satisfies another criteria desirable in an engineered matrix that it contain second phase particles, which are ductile at the application temperatures to enable ductile phase toughening.

Having demonstrated the validity of the proposed concept for designing engineered matrices, several new $CrSi_2$ and CrMoSi-based first generation engineered matrices were designed using either $CrSi_2$-SiC or CrMoSi-SiC as base compositions with additives to investigate their self-healing capabilities. Early results from the self-healing studies conducted on these matrices were encouraging. It was demonstrated that additions of 5(wt.%) CrB_2 to $CrSi_2$-SiC and CrMoSi-SiC matrices were effective in healing scratches and in partially closing ~1 mm diameter holes. These observations helped to downselect self-healing additives for formulating the compositions of the second generation engineered matrices.

References

1. D. Brewer, "HSR/EPM Combustor Materials Development Program," Mater. Sci. Eng. A, A261, (1999) 284–291.
2. C.M. Grondahl and T. Tsuchiya, "Performance Benefit Assessment of Ceramic Components in a MS9001FA Gas Turbine," J. Eng. Gas Turbine Power 123, (2000) 513–519.
3. T. Kameda, Y. Itoh, T. Hishata and T. Okamura, "Development of Continuous Fiber Reinforced Reaction Sintered Silicon Carbide Matrix Composite for Gas Turbine Hot Parts Application," ASME, (2000)2000-GT-67.
4. K.K. Chawla, "Ceramic Matrix Composites" (2nd ed.), Kluwer Academic Publishers, Norwell, MA, 2003.
5. G.S. Corman and K.L. Luthra, "Silicon Melt Infiltrated Ceramic Composites (HiPerComp)," *Handbook of Ceramic Composites* (edited by N. P. Bansal), Kluwer Academic Publishers, Boston, MA, 2005, pp. 99–115.
6. J.A. DiCarlo, H.M. Yun, G.N. Morscher and R.T. Bhatt, "SiC/SiC Composites for 1200 °C and Above," *Handbook of Ceramics, Glasses and Composites*, (edited by N. P. Bansal), Kluwer Academic Publishers, Boston, MA, pp. 77–98 (2005).
7. F. Christin, "CMC Materials for Space and Aeronautical Applications," *Ceramic Matrix Composites*, (edited by W. Krenkel), Wiley-VCH Verlag, 2008, pp. 327–351.

8. M.C. Halbig, M.H. Jaskowiak, J.D. Kiser and D. Zhu, "Evaluation of Ceramic Matrix Composite Technology for Aircraft Turbine Engine Applications". https://ntrs.nasa.gov/archive/nasa/casi.ntrs.nasa.gov/20130010774.pdf, 2013.
9. https://www.researchandmarkets.com/research/m3pjzn/global_ceramic, July 2017.
10. G.N. Morscher, "Stress-Dependent Matrix Cracking in 2D Woven SiC-Fiber Reinforced Melt-Infiltrated SiC Matrix Composites," Comp. Sci. Tech. 64 (2004) 1311–1319.
11. G.N. Morscher, M. Singh, J.D. Kiser, M. Freedman and R. Bhatt, "Modeling Stress-Dependent Matrix Cracking and Stress-Strain Behavior in 2D Woven SiC Fiber Reinforced CVI SiC Composites," Comp. Sci. Tech. 67 (2007) pp. 1009–1017.
12. G.N. Morscher and V.V. Pujar, "Design Guidelines for In-Plane Mechanical Properties of SiC Fiber-Reinforced Melt-Infiltrated SiC Composites," Int. J. Appl. Ceram. Technol. 6, (2009) 151–163.
13. G.N. Moscher, "Advanced Woven SiC/SiC Composites for High Temperature Applications," Composites at Lake Louise conference, Oct. 28-Nov. 2 (2007). https://ntrs.nasa.gov/archive/nasa/casi.ntrs.nasa.gov/20080006057.pdf, 2007.
14. S.V. Raj, "Thermal Expansion of Hot-Pressed Engineered Ceramic Materials," Ceramics International, 42 (2016) 2557–2569. http://dx.doi.org/10.1016/j.ceramint.2015.10.058.
15. C.A. Swenson, J. Phys. Chem. Ref. Data, 12 (1983) 179–182.
16. *Thermal Expansion: Nonmetallic Solids*, *Thermophysical Properties of Matter* (eds. Y.S. Touloukian, R.K. Kirby, R.E. Taylor and T.Y.R. Lee) vol. 13, Plenum, New York (1977) 1195–1220.
17. S.V. Raj, "Comparison of the Thermal Expansion Behavior of Several Intermetallic Silicide Alloys between 293 and 1523 K," J. Mater. Engineer. Perform.24 (2015)1199–1205. https://doi.org/10.1007/s11665-015-1390-8.
18. M.J. Maloney and R.J. Hecht, "Method for Improving Ceramic Fiber Reinforced Molybdenum Silicide Composites," US Patent 5,292,692 issued March 8, 1994.
19. M. Hebsur, Mater. Sci. Eng. A 261 (1999) 24–37.
20. S.V. Raj, "High Temperature Creep and Oxidation Resistant Chromium Silicide Matrix Alloy Containing Molybdenum," U. S. Patent No. 5,330,590 issued July 19, 1994.
21. S.V. Raj, "A Preliminary Assessment of the Properties of a Chromium Silicide Alloy for Aerospace Applications," Mater. Sci. Eng. A 192-193 (1995) 583–589.
22. S.V. Raj, Mater. Sci. Eng. A 201 (1995) 229–241.
23. R.M. Dickerson, S.V. Raj and I.E. Locci, "A Preliminary Investigation of the Cr_3Si -Mo Pseudo-Binary Phase Diagram, *Proceedings of the Materials Research Society*, Vol. 364, Materials Research Society, Pittsburgh, PA (1995) pp. 949–954.
24. S.V. Raj, J.D. Whittenberger, B. Zeumer and G. Sauthoff, "Elevated Temperature Deformation of Cr_3Si Alloyed with Mo," Intermetallics 7, (1999) 743–755.
25. ASTM C1161-02c, *Standard Test Method for Flexural Strength of Advanced Ceramics at Ambient Temperature*, ASTM International, West Conshohocken, PA, 2002. https://www.astm.org/doi.org/10.1520/C1161-02C.
26. ASTM C1211-13, *Standard Test Method for Flexural Strength of Advanced Ceramics at Elevated Temperatures*, ASTM International, West Conshohocken, PA, 2013. https:// www.astm.org/doi.org/10.1520/C1211.
27. S.V. Raj, unpublished research, NASA Glenn Research Center, Cleveland, OH (2015).
28. L.U.J.T. Ogbuji and E.J. Opila, "A Comparison of the Oxidation Kinetics of SiC and Si_3N_4," J. Electrochem. Soc. 142 (1995) 925–930.
29. O. Kubaschewski and B.E. Hopkins, "Oxidation of Metals and Alloys," Butterworths, London, 1967.
30. A.B. Gokhale and G.J. Abbaschian, *Binary Phase Diagrams* vol. 2 (eds. T. B. Massalski, H. Okamoto, P.R. Subramanian and L. Kacprzak) (1999) 1333–1335.